Journal of Solid Mechanics Vol. 13, No. 2 (2021) pp. 233-268
DOI: 10.22034/jsm.2020.1910389.1645

Iso-geometric Analysis for Topology Optimisation of Two Dimensional Planar and Laminated Composite Plate Continuum Structures

K.N.V. Chandrasekhar [1,*], V. Bhikshma [2], N. Rakesh [1], N. Swapnareddy [1], C. Rakesh[1]

[1]*Department of Civil Engineering, CVR College of Engineering, Hyderabad, Telangana, India*
[2]*University College of Engineering, Osmania University, Hyderabad, Telangana, India*

Received 13 March 2021; accepted 10 May 2021

ABSTRACT

Iso-geometric analysis is the recent development in the field of engineering analysis with high performance computing and greater precision. This current research has opened a new door in the field of structural optimisation. The main focus of this research study is to perform topology optimisation of continuum structures in civil engineering using Iso-geometric analysis. The continuum structures analysed here in this study are reinforced concrete, steel and laminated composite plates. Reinforced concrete is a rational union of concrete and steel. Topology optimisation of reinforced concrete structures is an emerging area of study to determine the optimal layout of material in the concrete domain. Laminated structures are made of several layers of material and bonded to achieve high stiffness and low weight to strength ratio. The deformed shape at the optimal state can be determined with topology optimisation of laminated composites. The formulation for composite plates is done using Kirchhoff thin plate theory without any shear contribution. B-splines are used to model the geometry. The objective is to optimise the energy of the structure and optimality criteria is used to calculate the newer values of relative densities. First order sensitivity analysis is performed to determine the newer values of objective function. The code is written in MATLAB® and a few problems have been solved with different domains. The results are verified and have shown a good agreement with those in the literature.

Keywords: Reinforced concrete; Iso-geometric; Topology; Optimisation; Laminates.

1 INTRODUCTION

REINFORCED concrete structure is a rational union of concrete and steel combined to act jointly. The joint action of concrete reinforced by steel bars in a reinforced concrete section will carry the loads and transfer them to the supports [1]. The arrangement of steel within the concrete has to address the nature and magnitude of the

*Corresponding author.
E-mail address: biml.koralla1@gmail.com (K.N.V. Chandrasekhar)

stresses produced within the material domain. This arrangement of steel has to be a valid arrangement and should have a rationale behind the arrangement. Several theories have been applied to design the arrangement of steel such as strut and tie model have been used in the past. The strut and tie model is a basic structure which is an idealisation of the given domain to carry the applied loads safely [2]. The strut and tie model is a truss model with struts carrying the compressive loads and ties carrying the tensile forces. The strut and tie models provide us with the basic understanding of the domain and its behavior under loading [3]. The strut and tie models can be prepared for a single loading. In case of multiple loads, the strut and tie models can be overlapped for each individual loading and a final form can be obtained. This becomes very repetitive and consumes lot of time and effort. Topology optimisation can be effectively useful in case of reinforced concrete domains carrying multiple loads. The optimisation process, evolutionary structural optimisation is performed with strain energy as the objective function. The elements which do not participate in the load carrying are gradually eliminated from the domain. The final distribution of material should be able to carry the given loading safely so that the stresses developed are well within the permissible limits [4]. Mohammed et.al. [5] did their study on optimisation of footing and retaining wall. Their research gave a modified Particle swarm optimisation (PSO) and compared the results with the previous studies which proves the validity and reliability of the algorithm. The objective of the study by James [6] is development of a new procedure to design reinforced concrete flat plate systems. The designs were compared with other flat plate modelling techniques including ACI direct design and equivalent frame techniques. Kwak and Filippou [7] did their study on motonic behavior of reinforced concrete beams slabs and beam-column joints sub assemblages. Concrete and steel are represented by different models which are combined together using a model to describe the combined behavior. The authors present a new procedure for layout design of reinforcement in concrete structures. Classical topology optimisation based on ground structure approach is applied to determine the optimal topology. Concrete is represented by a gradient enhanced continuous damage model and reinforcement is modeled as elastic bars embedded in concrete. Kaveh [8] present his work on optimal design of three dimensional multi-storied reinforced concrete building using charged system search, a meta-heuristic algorithm. The objective function is to minimise the weight of the structure. Pre-determined sections available are assumed for beams and columns and checked whether the section is acceptable or not. Kim and Baker [9] studied the optimisation of reinforced concrete structures using evolutionary structural optimisation. It accounts for bimaterial orthotropic nature of reinforced concrete by employing principal stress to drive optimisation. The optimisation formulation in his study also allows material to be added, optimising towards a fully stressed design. Oded amir [10] presented a gradient based continuum damage model for concrete and the reinforcement bars are embedded. Adjoint sensitivity analysis is derived in complete consistency with respect to path-dependency and the non-local model. Oded [11] presented in his model the reinforcement is represented by a set of all acceptable positions of rebars and are embedded into the continuum concrete domain. Both concrete and steel are designed simultaneously combining truss based and continuum-based methods. Oded Amir and Bogomolny [12] did their research study on computational procedure for optimal conceptual design of reinforced concrete structures based on topology optimisation with elastic-plastic material modelling. Several examples have been solved to illustrate the capability and potential of proposed procedure. Q.Q.Liang et.al.,[13] present performance based evolutionary topology optimisation to automate the optimal strut and tie model with displacement constraints. The element strain energy is calculated for element removal, while a performance index is used to monitor the evolutionary process. The optimal topology of strut and tie model is then determined. Several examples are solved to demonstrate the capability of the proposed method. Kamal and Adeli [14] presented a review of cost optimisation of concrete structures. These structures include beams, slabs, columns, frame structures, bridge, water tanks, folded plates, pipes, and shear walls and the important and interesting results are presented. Sara [15] did her study on artificial neural networks to perform cost optimisation of simply supported beams designed according to ACI-318-08 code. Computer models have been developed for structural optimisation of reinforced concrete structures using NEURO SHELL-2 software. Andres Guerra [16] presented the optimal sizing and reinforcing for beam and column members in multi-bay and multi-storey reinforced structures. A non-linear program searches for minimum cost solution that satisfies ACI code is used to perform the optimisation. Bikramjit [17] did his research work on optimisation of reinforced concrete doubly reinforced beams subjected to imposed loads.The design variables are taken as discrete variables to minimise the cost of the structure. Kaveh [18] presented big bang crunch algorithm to optimise reinforced concrete planar frames under gravity and lateral loads. The design is done according to ACI 318-08 code. Second order effects are also considered for compression members and column are checked for slenderness and end moments are magnified wherever necessary. Three building frames are optimised using big bang crunch algorithm and the results are compared with those obtained using genetic algorithm. Yousif [19] did his research on optimal design of continuous beams based on specifications of ACI satisfying the strength, serviceability, ductility, and durability. The dimensions of reinforcing bars are introduced as design variables considering flexure, shear and torsion effects on the beam. The optimum design results are in good

agreement with those in the literature. McCarthy and Cluskey [20] developed a new procedure to perform optimisation of reinforced concrete beams using particle swarm optimisation with multiple constraints following the specifications of Australian code 3600. Karthiga [21] presents finite element analysis of monotonic behavior reinforced concrete beams, slab and beam-column joint assemblages. Concrete and steel are represented as separate models which are combined together with an interaction between steel and concrete through bond-slip to describe the behavior of reinforced concrete composite material. The study has shown that the effect of tension stiffening and bond-slip are very important and should be included in finite element models of reinforced concrete structures. NSS and Chandrasekhar [22] did their work on step by step approach to analyse a two dimensional planar structure. The results of Iso-geometric analysis exactly matched with the results of finite element analysis. Chandrasekhar [23] presented his work on sizing optimisation of beams using Iso-geometric analysis. NSS and Chandrasekhar [24] presented their work on topology optimisation of continuum structures. The Michelle truss problem and a three-dimensional cube problem were analysed and optimised. The results obtained using Iso-geometric analysis were better than the optimisation results obtained by performing finite element analysis.

The recent developments in the field of materials has led to the invention of composite structures. These materials have been used in aerospace to civil engineering. Laminated structures are made in several layers and bonded to achieve high stiffness [25]. Laminated composites provide convenient design with tailor made layers, stacking sequence to obtain the design strength characteristics useful for several engineering applications. The analytical solutions can be obtained by using standard formulation to simple standard cases, but in real world complex problems needs complex analysis and solutions. There is a need to look for a analysis method which can provide us with accurate solutions [26]. Iso-geometric analysis is a recent computational approach that offers the possibility of giving solutions to complex problems. IGA offers the possibility of integrating the Nurbs based computer aided design tools with the finite element analysis. This comes from the family of meshless methods and overcome the drawback of finite element method [27].The surfaces can be represented using higher order polynomials and construct the shape of the structure. In the present formulation, cubic order polynomials are used with C^2 continuity condition. A mesh for a Nurbs patch is formed by the product of knot vectors. The knots divide the design domain into elements. The control points are associated with the the basis functions that define the geometry. The boundary conditions can be applied to the control points [28]. Accurate modeling and prediction of the response of the laminated structures is a complex task because the composite laminates are orthotropic in nature. Meshless methods for the analysis of laminated plates are gaining increasing interest because of higher order approximation and refinement to obtain accurate results [29]. The formulation used here is classical laminated plate theory known as Kirchoff theory of thin plates [30]. Dufour et.al. [31] proposed a 3D geometric based method to study the variation of stress through the thickness. This method used a C^0 continuity of each ply of the laminate. The results have shown a good agreement when applied on slender composite stacks with a large number of layers. The method proves computationally effective over traditional layer wise methods and where the researchers are looking for better alternatives, this method proves to be an alternate solution. Navid et.al. [32] in his study on functionally graded plates, has used NURBS and performed static, vibration, buckling analysis. The material properties are assumed to be graded in the thickness direction and the effective properties are computed using Mori-Tanaka scheme. The solution obtained has shown good agreement with the three dimensional analytical solution. A detailed numerical study has been performed to study the influence of gradient index, plate thickness and plate aspect ratios and determine the global response of the laminate. Xuan et.al. [33] did his study on buckling analysis of generally laminated composite beam with various boundary conditions. The model is detailed by applying the principle of virtual work. Numerical results of critical buckling loads and mode shapes are presented. The impact of modulus ratios, fibre angles, stacking sequence and slenderness ratio on the critical buckling effects are evaluated. The results have shown a good agreement with those in the literature. Madhukar and Amirtham [34] did their research on bending and vibration analysis of plates and laminates. They presented meshless natural Galerkin method to take the advantage of geometric flexibility of meshless method. The nodal connectivity is imposed on nodal sets with reduced size, reducing significantly the computational effort required to construct shape functions. Several numerical examples are presented to demonstrate the efficacy of the present method to calculate stresses, deflections. Weeger et.al. [35] presented a novel approach of isogeometric finite elements. A non-linear framework based on the harmonic balance principle is used here in their study on non-linear Euler Bernouli beam vibrations. They demonstrated that Isogeometric finite elements with B-Splines in combination with harmonic balance method gave good results. Alessia et.al. [36] did their study on using Isogeometric collocation method over Galerkin method to reduce the computational effort. The plates are modelled with one element through the thickness to guarantee the results of in-plane stress components. The continuity demand is fully met and excellent results are obtained using a minimal number of collocation points per direction. Saeed et.al. [37] used isogeometric finite element method to perform free vibration and buckling analysis of laminated composite plates. The essential boundary conditions are

formulated separately using Lagrange multiplier method, while an orthogonal transformation technique is applied to impose boundary conditions. Several problems have been solved with different boundary conditions, fibre orientation, eigen modes to check the efficiency of the proposed method. The results obtained are in good agreement with the analytical method or other numerical methods in the literature. Amir and Mohammad [38] present their study on optimisation of laminated plates using NURBS to model the geometry and to calculate the field variables. Boundary conditions are imposed using collocation method. A few examples are evaluated using proposed method and verified using element free Galerkin and theoretical method. The optimisation of orientation, number and stacking sequence of lamina is performed using genetic algorithm with a multi-objective structural optimisation problem. Chien et.al. [39] did their study on composite laminate sandwich plates using classical laminate plate theory and Iso-geometric analysis. B-Splines can be used to approximate geometry and displacements and provide a flexible way to perform degree elevation and refinement. In the present formulation, only non-dimensional displacement is evaluated at each control point. Several numerical examples are illustrated to check the performance of the present method with other published methods. Farshad and Roger [40] did their research on non-linear shell elements. They proposed two formulations for modelling thin laminated composite shells. The composite shell is modelled in the framework of equivalent single layer theory. The solution is obtained using quadratic NURBS based elements to ensure the smoothness required for analysis of thin shells. The accuracy of the proposed method is verificed with several numerical examples. Shuang [41] did his study on multi-level optimisation of laminated composite thin-walled structures. The aim of this research is to apply the iso-geometric analysis to the multilevel optimisation design. This new method has high efficiency and high safety for industrial design of thin-walled structures. Hitesh [42] did his research on composite structures and developed code to perform stress analysis of composite and sandwich beams and plates. Nurbs based Iso-geometric analysis both linear and non-linear code is developed for static and dynamic analysis of laminated composite plates. Stress analysis of plates with a hole and stress concentration factor is calculated. The results are in good agreement with those obtained in the literature using other methods. Abha and Anup [43] did their study on thermo-elastic behavior of laminated sandwich composite plates. They used iso-geometric analysis to perform a parametric study with quadratic, cubic and quartic NURBS elements with respect to temperature. Changes in deflections, stresses and moment resultants are analysed with an aim to understand the response of laminated composite plate. Several examples have been solved and the results are compared with those existing in the literature and validate. Cesar [44] in his research work on composites focusses on two areas pertaining to the field of structural analysis and other within the field of structural health monitoring. His work is divided into two parts. The first portion is focused on Nurbs based analysis of composites. The second part is in the field of delamination detection in carbon fibre reinforced polymer plates. Several numerical and experimental analysis are performed to study the delamination detection through the use of piezo-electric sensors and actuators. They have used a 4-node quadrilateral delaminated composite plate element for damage detection. Mode shape changes, frequency shifts, frequency response function changes are computed to study the effect of delamination. Josef [45] in his research work on shape optimisation of shell structures using Iso-geometric analysis. Another co-operation project with the structural formulation integrated with the environment and is applied to a three dimensional simulation of a wind turbine blade rotating in air flow. This example shows how the application to large industrial structures can be performed. Loc et.al. [46] did their research work on Isogeometric analysis with third order shear deformation theory for thermal buckling of composite laminates. TSDT accounts for shear deformation without shear correction factor. The material properties of plates are assumed to vary according to power law distribution of volume fraction of constituents. The temperature field through the plate thickness is described by polynomial series. Numerical results of circular and rectangular plates are provided to validate the proposed model. Vinh Loc [47] did his research work on composite laminates using higher order shear deformation theory and Iso-geometric analysis. His work is divided into four parts. Firstly, bending analysis using HSDT models secondly the elastic instability behavior of functionally graded plates under in-plane comparision load is investigated. Thirdly, dynamic problems related to free and forced vibrations are solved. Finally , cracked plates are modelled and analysed using general shear deformation theory. Michael et. al. [48] in his work prevented a new method to determine the optimal segmentation of shell structures built from precast patches made from fibre reinforced concrete using iso-geometric analysis. The procedure is integrated with Rhino3D and successfully demonstrated. Iso-geometric analysis is applied with a damage model to simulate progressive failures by X.Deng [49]. The proposed methodology is valid for thin shells where damage occurs without significant delamination. The results are validated against experimental data in the context of composite damage analysis. Kiani [50] presented his study on thermal post-buckling analysis for composite laminated plates reinforced with graphene sheets. He used third order shear deformation plate theory. The material properties are estimated by refined Haptin-Tsai approach which contains efficiency parameters. Thermally induced post buckling curves of composite plate reinforced by graphene are provided for different aspect ratios, side to thickness, boundary conditions. They found

that *X*-pattern of graphene reinforcement results in highest load and least post-buckling deflection. Pavan and Mallikarjun [51] did their study on Iso-geometric collocation methods to perform the analysis using Reissner-Mindlin plate theory. The collocation method discretises the governing equation in strong form and retain inherent IGA features by using Non-uniform rational B-Splines. H.Liu [52] presented his work on IGA-SIMP method for stress-constrained topology optimisation. He formulated the optimisation problem as a minimisation problem under maximum Von-Mises stress constraint. He compared the stress obtained using IGA and FEA. He presented several examples using bi-linear quadratic elements and optimised using IGA-SIMP method. The results obtained using the proposed method IGA-SIMP are in good agreement with those given in the literature. Omer [53] in his research presented the geometrically nonlinear static analysis of thin rectangular plates on Winkler-Pasternak elastic foundation. The differential equations have been solved using discrete single convolution method. The geometry of a typical rectangular plate resting on Winkler elastic foundation is modeled and the governing equations are derived. The effect of boundary conditions is studied on the response of the structure measured in terms of the deflections. The parameters *K* and *G* of the Winkler and Pasternak foundation has been found to have significance influence on the displacements of the plates. Omer and Okyay [54] applied discrete singular convolution method for numerical solution of the equation of motion of Timoshenko beam. The effect of different boundary conditions is studied in detail. They studied the variation of frequency with h/L ratios for several boundary conditions and they found that they effect is more visible in higher modes than in the first mode when the ratio of *h/L* is higher. DSC is important for large-scale computations and is a promising approach for computational mechanics. Bekir Akgoz and Omer Civalek[55] presented their study on microstructure-dependent buckling behavior of single-walled carbon nanotubes surrounded by a two-parameter elastic foundation. They performed a parametric study to indicate the effects of diameter-t_0-length ratio, shear deformation, shear correction factor and foundation parameters on buckling loads of single walled carbon nano tubes. Higher order shear deformation theory is used in this study. It is found that the classical normalised buckling loads corresponding to all shear deformation theories is nearly equal to one for smaller *D/L* but as the ratio of *d/L* increases there is a decrement in the normalised buckling loads. Shear deformation is more significant on the buckling loads for shorter carbon nanotubes. Helong et.al. [56] did their research on thermo-mechanical parametric instability of functionally graded multilayer GPLRC plates under a periodic uniaxial force with a uniform rise in temperature. Shen et.al. [57] did their study on nonlinear vibration behavior of uniformly distributed and functionally graded graphene reinforced laminated cylindrical panels. A parametric study is conducted and they determined that the ratio of nonlinear to linear frequency ratios are increased by increasing the temperature.

Section 1 discussed the existing literature on the optimisation of reinforced concrete structures. In the section 2, the theoretical background on Isogeometric analysis is presented. Section 3, the flowchart showing the approach followed to conduct this study. The assumptions made are stated here. In section 4, several problems having different reinforced concrete domain have been analysed and the optimal results are discussed. In the section 5, the static analysis is performed and the results are compared with those given in the literature. In section 6, the topology optimisation of simply supported laminated composite square plate is performed for four different lamina. In section 7, the conclusions are presented and the future scope of the study is given. Towards the end of the paper, the references followed to conduct this study are given in order.

Objectives of the study:

1. To model and analyse the reinforced concrete structures using Isogeometric analysis.
2. To perform topology optimisation with compliance as the objective function using cubic B-splines and determine the optimal distribution of material.
3. To plot the stress distribution for the optimal distribution of material within the material domain.
4. To determine the performance index of the optimal distribution based on Compliance.
5. To perform topology optimisation of SSSS laminated composite plates using cubic B-splines subjected to sinusoidal loading.

Scope of the study:

1. The study is valid within the linear static elastic limits only.
2. Hooke's law is valid.
3. The study does not include buckling analysis.
4. The effect of temperature and moisture are not included in the analysis.
5. The age of reinforced concrete material is not included in the analysis.

2 THEORETICAL BACKGROUND

In the previous section, the literature review has been done. In this section, the theory and the formulation necessary to analyse the given domain using Iso-geometric analysis is presented here.

2.1 Connectivity analysis [58]

Connectivity analysis will identify all the elements above the threshold value and also has a face connectivity with other elements connecting all the seed elements within the given continuum. In other words, all the elements having an edge or a corner connectivity and/or not connected will be assigned a very small density value equal to 1e-5 during the analysis. The Fig. 1(a) shows an example of elements that are not connected and Fig. 1(b) shows two elements connected with a face connectivity in common.

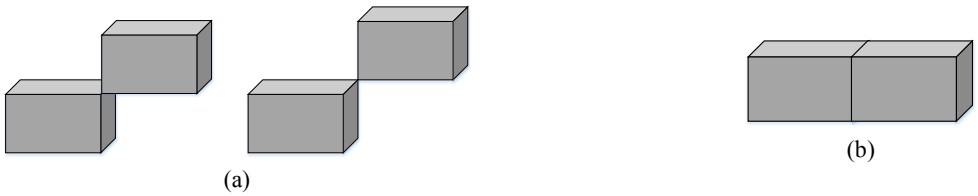

Fig.1
(a) Elements not connected. (b) Elements connected - Face connectivity.

FE analysis is performed using a constant meshing technique in which all the elements in the structure will be considered during the analysis and all the elements without connectivity are assigned a lower density value of 1*e*-5.

2.2 Theory behind the knot vectors

The theory behind the knot vectors for a quadratic and a cubic curve are given here.

2.2.1 Quadratic

For degree of the curve is $p = 2$, the support is over p+1 knot spans. The knot vector of p+1+1 knots is required to calculate the basis functions.

The element is defined using a knot span and the basic functions are valid for a knot span. The knot span is different for each element and the corresponding basis functions have to be calculated separately for each element. For example, p=2 and knot vector is {0, 0, 0, 1/4, 2/4, 3/4, 4/4, 4/4, 4/4}. The number of local knots is equal to four per element, which means that the basis functions are (N_1 N_2 N_3) as shown in Table 1.

Table 1
For p=2, the local knot vector per element.

Local knot vector	Greville Points for Identity parameterization only
0 0 0 1/4	0.5 * (0+0) = 0
0 0 1/4 2/4	0.5 * (0+1/4) = 1/8
0 1/4 2/4 3/4	0.5 * (1/4+1/2) = 3/8
1/4 2/4 3/4 1	0.5 * (1/2+3/4) = 5/8
2/4 3/4 1 1	0.5 * (3/4+1) = 7/8
3/4 1 1 1	0.5 * (1+1) = 1

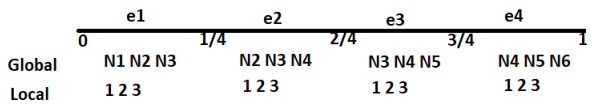

Fig.2
The number of local knots for the quadratic curve.

The IGA elements are rotation free elements. The continuity can be maintained by having knots in common in Fig.2. For a quadratic degree, we have two in common and for a cubic degree curve we have three in common.

2.2.2 Cubic curve

For degree of the curve is $p = 3$, the support is over p+1 knot spans. The knot vector of p+1+1 knots is required to calculate the basis functions. The element is defined using a knot span and the basis functions are valid for a knot span.

The knot span is different for each element and the corresponding basis functions have to be calculated separately for each element. For example, p=3 and knot vector is {0, 0, 0, 0, 1/4, 2/4, 3/4, 4/4, 4/4, 4/4, 4/4}. The number of knots is equal to five per element, which means that the basis functions are (N_1 N_2 N_3 N_4) as shown in Table 2.

Table 2
For p=3, the local knot vector per element.

Local knot vector	Greville Points for identity parameterization only
0 0 0 0 1/4	(1/3) * (0+0+0) = 0
0 0 0 1/4 2/4	(1/3) * (0+0+1/4) = 1/12
0 0 1/4 2/4 3/4	(1/3) * (0+1/4+1/2) = 1/4 = 3/12
0 1/4 2/4 3/4 1	(1/3) * (1/4+1/2+3/4) = 1/2 = 6/12
1/4 2/4 3/4 1 1	(1/3) * (2/4+3/4+1) = 3/4 = 9/12
2/4 3/4 1 1 1	(1/3) * (3/4+1+1) = 11/12
3/4 1 1 1 1	(1/3) * (1+1+1) = 12/12

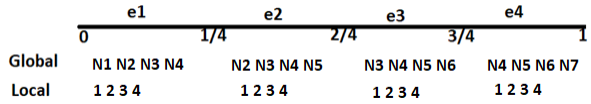

Fig.3
The number of local knots for a cubic curve.

The IGA elements are rotation free elements. The continuity can be maintained by having knots in common in Fig.3. For a quadratic degree, we have two in common and for a cubic degree curve we have three in common. The problems in structural mechanics requires control points to be defined at the points where deflection has to be calculated. The control points can be defined at equal intervals over the entire length of the beam. The behavior can be non-linear in such cases.

2.3 Nurbs formulation

The basic theory is discussed in this section. The NURBS basis functions and the parent to parametric mapping are discussed. The strain displacement matrix is presented and then form the stiffness matrix. Chandrasekhar [23] presents an example of a two-dimensional plate continuum is analysed using Iso-geometric analysis. The NURBS basis functions are used and are discussed first. The stiffness matrix is derived in a step wise manner. The solution for the displacement vector at each node is compared with the results from the standard finite element analysis. The results show that the nodal displacement is in good agreement with the results obtained from IGA and the nodal displacements using standard FEA.

2.3.1 Basis functions [24]

The basis functions are given by

$$N_{i,0}(\xi) = \begin{Bmatrix} 1 & if \;\; \xi_i \le \xi < \xi_{i+1} \\ 0 & otherwise \end{Bmatrix}$$

For p = 1, 2, 3, …. They are defined by

$$N_{i,p}(\xi)=\frac{\xi-\xi_i}{\xi_{i+p}-\xi_i}N_{i,p-1}(\xi)+\frac{\xi_{i+p+1}-\xi}{\xi_{i+p+1}-\xi_{i+1}}N_{i+1,p-1}(\xi) \tag{1}$$

This is referred to as the Cox-de Boor recursion formula.
Derivatives of B-Spline Basis functions. The derivatives of the basis functions are given by

$$\frac{d}{d\xi}N_{i,p}(\xi)=\frac{p}{\xi_{i+p}-\xi_i}N_{i,p-1}(\xi)-\frac{p}{\xi_{i+p+1}-\xi_{i+1}}N_{i+1,p-1}(\xi)$$

Generalize to higher order derivatives [59]. The generalized higher order derivatives of the basis functions is given by

$$\frac{d^k}{d^k\xi}N_{i,p}(\xi)=\frac{p}{\xi_{i+p}-\xi_i}\left(\frac{d^{k-1}}{d^{k-1}\xi}N_{i,p-1}(\xi)\right)-\frac{p}{\xi_{i+p+1}-\xi_{i+1}}\left(\frac{d^{k-1}}{d^{k-1}\xi}N_{i+1,p-1}(\xi)\right) \tag{2}$$

B-spline curves. The B-spline curve is given by

$$C(\xi)=\sum_{i=1}^{n}N_{i,p}(\xi)P_i$$

B-spline surfaces. B-spline surfaces is given by

$$S(\xi,\eta)=\sum_{i=1}^{n}\sum_{j=1}^{m}N_{i,p}(\xi)M_{j,q}(\eta)P_{i,j} \tag{3}$$

B-spline solids. B-spline solids is given by

$$S(\xi,\eta,\varsigma)=\sum_{i=1}^{n}\sum_{j=1}^{m}\sum_{k=1}^{l}N_{i,p}(\xi)M_{j,q}(\eta)L_{k,r}(\varsigma)P_{i,j,k}$$

2.4 Performance index

Liang [60] in his work on Performance based topology optimisation of reinforced concrete structures presents the measures of performance of the structure based on compliance of the structure.

If W_0 denotes the weight of the structure and W_i denotes the weight of structure in each iteration. If C_0 denotes the compliance of the structure and C_i denotes the compliance of the structure at each iteration. Performance index of the structure is defined as:

$$PI=\frac{W_0}{W_i}*\frac{C_0}{C_i} \tag{4}$$

The performance index of the structure indicates the non-dimensional measure of the efficiency of the structure in carrying the load and transfer to the supports effectively.

2.5 Formulation of laminated plates

Let Ω be the domain in R^2 by the mid plane of the plate and *u, v, w* denote the displacement components in *x, y, z* directions respectively. Using the Kirchoff theory [61] the displacements at any point can be expressed as:

$$\begin{aligned} u(x,y,z) &= u_o(x,y) - z\,\theta_x(x,y) \\ v(x,y,z) &= v_o(x,y) - z\,\theta_y(x,y) \\ w(x,y,z) &= w(x,y) \end{aligned} \tag{5}$$

where, $\theta_x = \dfrac{\partial w}{\partial x}$ and $\theta_y = \dfrac{\partial w}{\partial y}$. In-plane strains through the following equation

$$\varepsilon = \left[\varepsilon_{xx}, \varepsilon_{yy}, \gamma_{xy}\right]^T = \varepsilon_o + z\,\kappa$$

where, ε_o, κ are the in-plane deformations and curvatures of the middle surface respectively

$$\varepsilon_o = \begin{bmatrix} \dfrac{\partial}{\partial x} & 0 & 0 \\ 0 & \dfrac{\partial}{\partial y} & 0 \\ \dfrac{\partial}{\partial y} & \dfrac{\partial}{\partial x} & 0 \end{bmatrix} \begin{bmatrix} u_o \\ v_o \\ w \end{bmatrix} \quad and \quad \kappa = \begin{bmatrix} 0 & 0 & -\dfrac{\partial^2}{\partial x^2} \\ 0 & 0 & -\dfrac{\partial^2}{\partial y^2} \\ 0 & 0 & -2\dfrac{\partial^2}{\partial x\,\partial y} \end{bmatrix} \begin{bmatrix} u_o \\ v_o \\ w \end{bmatrix} \tag{6}$$

$$\begin{aligned} \overline{Q}_{11} &= Q_{11}\cos^4\theta + 2(Q_{12}+2Q_{66})\sin^2\theta\cos^2\theta + Q_{22}\sin^4\theta \\ \overline{Q}_{12} &= (Q_{11}+Q_{22}-4Q_{66})\sin^2\theta\cos^2\theta + Q_{12}(\sin^4\theta+\cos^4\theta) \\ \overline{Q}_{16} &= (Q_{11}-Q_{12}-2Q_{66})\sin\theta\cos^3\theta + (Q_{12}-Q_{22}+2Q_{66})\sin^3\theta\cos\theta \\ \overline{Q}_{22} &= Q_{11}\sin^4\theta + 2(Q_{12}+2Q_{66})\sin^2\theta\cos^2\theta + Q_{22}\cos^4\theta \\ \overline{Q}_{26} &= (Q_{11}-Q_{12}-2Q_{66})\sin^3\theta\cos\theta + (Q_{12}-Q_{22}+2Q_{66})\sin\theta\cos^3\theta \\ \overline{Q}_{66} &= (Q_{11}+Q_{22}-2Q_{12}-2Q_{66})\sin^2\theta\cos^2\theta + Q_{66}(\sin^4\theta+\cos^4\theta) \end{aligned}$$

with

$$\begin{aligned} &Q_{11} = \frac{E_{11}}{1-\upsilon_{12}\upsilon_{21}}, \quad Q_{12} = \frac{\upsilon_{12}E_{11}}{1-\upsilon_{12}\upsilon_{21}}, \quad Q_{22} = \frac{E_{22}}{1-\upsilon_{12}\upsilon_{21}}, \\ &Q_{44} = G_{13}, \qquad Q_{55} = G_{23}, \qquad Q_{66} = G_{12} \end{aligned}$$

$$\upsilon_{21}E_{11} = \upsilon_{12}E_{22} \tag{7}$$

E_{11} and E_{22} are Young's modulus of elasticity parallel and perpendicular to the fibre orientation. G_{12} is the shear modulus and are υ_{12} and υ_{21} are Poisson's' ratios [62]. As shown in the Fig.4, the layers of lamina are given, the distance is measured from the centre of the lamina.

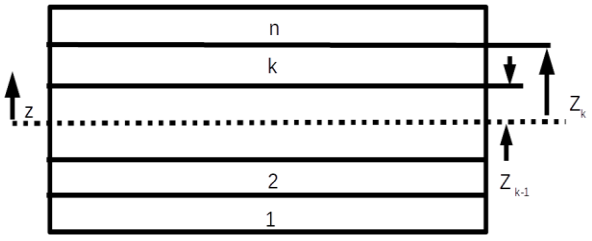

Fig.4
Showing the layers of lamina.

$$[E]=\begin{bmatrix} A_{11} & A_{12} & A_{16} & B_{11} & B_{12} & B_{16} \\ A_{21} & A_{22} & A_{26} & B_{21} & B_{22} & B_{26} \\ A_{61} & A_{62} & A_{66} & B_{61} & B_{62} & B_{66} \\ B_{11} & B_{12} & B_{16} & D_{11} & D_{12} & D_{16} \\ B_{21} & B_{22} & B_{26} & D_{21} & D_{22} & D_{26} \\ B_{61} & B_{62} & B_{66} & D_{61} & D_{62} & D_{66} \end{bmatrix}=\begin{bmatrix} A & B \\ B & D \end{bmatrix}$$

$$\begin{aligned} A_{ij} &= \sum_{k=1}^{n}\left(\overline{Q}_{ij}\right)_k \left(z_k - z_{k-1}\right) \qquad & B_{ij} &= \frac{1}{2}\sum_{k=1}^{n}\left(\overline{Q}_{ij}\right)_k \left(z_k^2 - z_{k-1}^2\right) \\ D_{ij} &= \frac{1}{3}\sum_{k=1}^{n}\left(\overline{Q}_{ij}\right)_k \left(z_k^3 - z_{k-1}^3\right) \qquad & i, j &= 1,2,6 \end{aligned} \tag{8}$$

The value of z is measured from the centre of the lamina as shown in the Fig.4. Using the NURBS basis functions, both the description of the geometry for the physical and the displacement field are expressed as:

$$x^h(\xi,\eta) = \sum_{A}^{nm} R_A(\xi,\eta) P_A$$

$$u^h(x(\xi,\eta)) = \sum_{A}^{nm} R_A(\xi,\eta) q_A$$

where, *n, x, m* is the number of basic functions.

$x^T = (x \quad y)$ is the physical coordinate vector, $R_A(\xi,\eta)$ is rational basic functions and $q_A = \left[u_A \; v_A \; w_A\right]^T$ is the degrees of freedom of u^h associated to the control point A.

The strains can be expressed to following nodal displacements as:

$$\left[\varepsilon_o \quad \kappa\right]^T = \sum_{A}^{nm}\left[B_A^m \; B_A^b\right]^T q_A$$

$$B_A^m = \begin{bmatrix} R_{A,x} & 0 & 0 \\ 0 & R_{A,y} & 0 \\ R_{A,y} & R_{A,x} & 0 \end{bmatrix} \text{ and } B_A^b = \begin{bmatrix} 0 & 0 & -R_{A,xx} \\ 0 & 0 & -R_{A,yy} \\ 0 & 0 & -2R_{A,xy} \end{bmatrix}$$

B_A^m and B_A^b are membrane and bending strain displacement matrices using the derivatives of the basis function [62]. Global stiffness matrix $\mathbf{K} = \int_{\Omega}\left\{\begin{bmatrix}\mathbf{B}^m \\ \mathbf{B}^b\end{bmatrix}^T \begin{bmatrix}\mathbf{A} & \mathbf{B} \\ \mathbf{B} & \mathbf{D}\end{bmatrix}\begin{bmatrix}\mathbf{B}^m \\ \mathbf{B}^b\end{bmatrix}\right\} d\Omega$. Force vector is

$$f = \int_{\Omega} pR\, d\Omega \tag{9}$$

For sinusoidal loading, $p = p_0 \sin(\pi x / a)\sin(\pi y / b)$. $\boldsymbol{q}$ is the global displacement vector

2.6 Derivation for second derivative

We know that

$$\begin{bmatrix} \frac{dN}{dx} \\ \frac{dN}{dy} \end{bmatrix} = \begin{bmatrix} \frac{dx}{d\xi} & \frac{dy}{d\xi} \\ \frac{dx}{d\eta} & \frac{dy}{d\eta} \end{bmatrix}^{-1} \begin{bmatrix} \frac{dN}{d\xi} \\ \frac{dN}{d\eta} \end{bmatrix} \tag{10}$$

$$\frac{dN}{d\xi} = \frac{dN}{dx}\frac{dx}{d\xi} + \frac{dN}{dy}\frac{dy}{d\xi} \tag{11}$$

Differentiating w.r.t. ξ

$$\frac{d^2N}{d\xi^2} = \frac{d}{d\xi}\left(\left(\frac{dN}{dx}\right)\frac{dx}{d\xi}\right) + \frac{d}{d\xi}\left(\left(\frac{dN}{dy}\right)\frac{dy}{d\xi}\right)$$

$$P = \frac{dN}{dx} \qquad Q = \frac{dN}{dy}$$

$$\frac{d^2N}{d\xi^2} = \left(\frac{dP}{dx}\frac{dx}{d\xi} + \frac{dP}{dy}\frac{dy}{d\xi}\right)\frac{dx}{d\xi} + \left(\frac{dQ}{dx}\frac{dx}{d\xi} + \frac{dQ}{dy}\frac{dy}{d\xi}\right)\frac{dy}{d\xi} + \frac{dN}{dx}\frac{d^2x}{d\xi^2} + \frac{dN}{dy}\frac{d^2y}{d\xi^2}$$

$$\frac{d^2N}{d\xi^2} = \frac{d^2N}{dx^2}\left(\frac{dx}{d\xi}\right)^2 + \frac{d^2N}{dxdy}\frac{dx}{d\xi}\frac{dy}{d\xi} + \frac{d^2N}{dxdy}\frac{dx}{d\xi}\frac{dy}{d\xi} + \frac{d^2N}{dy^2}\left(\frac{dy}{d\xi}\right)^2 + \frac{dN}{dx}\frac{d^2x}{d\xi^2} + \frac{dN}{dy}\frac{d^2y}{d\xi^2}$$

$$\frac{d^2N}{dx^2}\left(\frac{dx}{d\xi}\right)^2 + 2\frac{d^2N}{dxdy}\frac{dx}{d\xi}\frac{dy}{d\xi} + \frac{d^2N}{dy^2}\left(\frac{dy}{d\xi}\right)^2 = +\frac{d^2N}{d\xi^2} - \frac{dN}{dx}\frac{d^2x}{d\xi^2} - \frac{dN}{dy}\frac{d^2y}{d\xi^2}$$

Similarly,

$$\frac{d^2N}{dx^2}\left(\frac{dx}{d\eta}\right)^2 + 2\frac{d^2N}{dxdy}\frac{dx}{d\eta}\frac{dy}{d\eta} + \frac{d^2N}{dy^2}\left(\frac{dy}{d\eta}\right)^2 = +\frac{d^2N}{d\eta^2} - \frac{dN}{dx}\frac{d^2x}{d\eta^2} - \frac{dN}{dy}\frac{d^2y}{d\eta^2}$$

Differentiating Eq.(23) w.r.t. η

$$\frac{d^2N}{d\eta d\xi} = \frac{d}{d\eta}\left(\left(\frac{dN}{dx}\right)\frac{dx}{d\xi}\right) + \frac{d}{d\eta}\left(\left(\frac{dN}{dy}\right)\frac{dy}{d\xi}\right)$$

$$\frac{d^2N}{d\eta d\xi} = \left(\frac{dP}{dx}\frac{dx}{d\eta} + \frac{dP}{dy}\frac{dy}{d\eta}\right)\frac{dx}{d\xi} + \left(\frac{dQ}{dx}\frac{dx}{d\eta} + \frac{dQ}{dy}\frac{dy}{d\eta}\right)\frac{dy}{d\xi} + \frac{dN}{dx}\frac{d^2x}{d\eta d\xi} + \frac{dN}{dy}\frac{d^2y}{d\eta d\xi}$$

$$\frac{d^2N}{d\eta d\xi} = \frac{d^2N}{dx^2}\frac{dx}{d\eta}\frac{dx}{d\xi} + \frac{d^2N}{dydx}\frac{dy}{d\eta}\frac{dx}{d\xi} + \frac{d^2N}{dxdy}\frac{dx}{d\eta}\frac{dy}{d\xi} + \frac{d^2N}{dy^2}\frac{dy}{d\eta}\frac{dy}{d\xi} + \frac{dN}{dx}\frac{d^2x}{d\eta d\xi} + \frac{dN}{dy}\frac{d^2y}{d\eta d\xi}$$

$$\frac{d^2N}{dx^2}\frac{dx}{d\eta}\frac{dx}{d\xi} + \frac{d^2N}{dydx}\frac{dy}{d\eta}\frac{dx}{d\xi} + \frac{d^2N}{dxdy}\frac{dx}{d\eta}\frac{dy}{d\xi} + \frac{d^2N}{dy^2}\frac{dy}{d\eta}\frac{dy}{d\xi} = \frac{d^2N}{d\eta d\xi} - \frac{dN}{dx}\frac{d^2x}{d\eta d\xi} - \frac{dN}{dy}\frac{d^2y}{d\eta d\xi}$$

$$\begin{bmatrix} \left(\frac{dx}{d\xi}\right)^2 & \left(\frac{dy}{d\xi}\right)^2 & 2\frac{dx}{d\xi}\frac{dy}{d\xi} \\ \left(\frac{dx}{d\eta}\right)^2 & \left(\frac{dy}{d\eta}\right)^2 & 2\frac{dx}{d\eta}\frac{dy}{d\eta} \\ \frac{dx}{d\eta}\frac{dx}{d\xi} & \frac{dy}{d\eta}\frac{dy}{d\xi} & \frac{dx}{d\eta}\frac{dy}{d\xi} + \frac{dy}{d\eta}\frac{dx}{d\xi} \end{bmatrix} \begin{bmatrix} \frac{d^2N}{dx^2} \\ \frac{d^2N}{dy^2} \\ \frac{d^2N}{dxdy} \end{bmatrix} = \begin{bmatrix} \frac{d^2N}{d\xi^2} - \frac{dN}{dx}\frac{d^2x}{d\xi^2} - \frac{dN}{dy}\frac{d^2y}{d\xi^2} \\ \frac{d^2N}{d\eta^2} - \frac{dN}{dx}\frac{d^2x}{d\eta^2} - \frac{dN}{dy}\frac{d^2y}{d\eta^2} \\ \frac{d^2N}{d\eta d\xi} - \frac{dN}{dx}\frac{d^2x}{d\eta d\xi} - \frac{dN}{dy}\frac{d^2y}{d\eta d\xi} \end{bmatrix} \tag{12}$$

$$\begin{bmatrix} \frac{d^2N}{dx^2} \\ \frac{d^2N}{dy^2} \\ \frac{d^2N}{dxdy} \end{bmatrix} = \begin{bmatrix} \left(\frac{dx}{d\xi}\right)^2 & \left(\frac{dy}{d\xi}\right)^2 & 2\frac{dx}{d\xi}\frac{dy}{d\xi} \\ \left(\frac{dx}{d\eta}\right)^2 & \left(\frac{dy}{d\eta}\right)^2 & 2\frac{dx}{d\eta}\frac{dy}{d\eta} \\ \frac{dx}{d\eta}\frac{dx}{d\xi} & \frac{dy}{d\eta}\frac{dy}{d\xi} & \frac{dx}{d\eta}\frac{dy}{d\xi}+\frac{dy}{d\eta}\frac{dx}{d\xi} \end{bmatrix}^{-1} \begin{bmatrix} \frac{d^2N}{d\xi^2}-\frac{dN}{dx}\frac{d^2x}{d\xi^2}-\frac{dN}{dy}\frac{d^2y}{d\xi^2} \\ \frac{d^2N}{d\eta^2}-\frac{dN}{dx}\frac{d^2x}{d\eta^2}-\frac{dN}{dy}\frac{d^2y}{d\eta^2} \\ \frac{d^2N}{d\eta d\xi}-\frac{dN}{dx}\frac{d^2x}{d\eta d\xi}-\frac{dN}{dy}\frac{d^2y}{d\eta d\xi} \end{bmatrix} \tag{12}$$

3 APPROACH

Continuum optimisation problems are usually classified as NP Hard Problems, which mean non-deterministic polynomial problems which usually cannot be solved manually [63]. The objective here is to perform topology optimisation of continuum structures using Isogeometric analysis instead of applying finite element analysis. The topology optimisation as shown in the Fig.4 is one of the important steps in the Integrated optimisation process in order to arrive at a final layout of the material distribution. Integrated optimisation [5960] process involves several stages. The process begins with problem definition where in the real time need of the design is clearly defined. The physical aspects of the problem is identified, the four properties of the domain namely the geometry, the material properties, the forces acting and the support conditions are identified. The formulation of the problem, and the assumptions involved are identified at this stage. The next phase of the integrated optimisation is boundary smoothing which is done using Auto CAD. The topology output is refined and is given a definite shape and dimensions. The final model from Auto CAD is then used to reconstruct the solid model which is normally done using a finite element analysis package namely Solid Works ® from Dassault systems (DSS). The solid model is analysed to check for permissible stresses and displacements. Upon successful analysis, the shape optimisation of the solid model can be performed using Design Works, a commercial package. The final distribution of material design can then be sent to the casting division for a prototype.

The main focus of this study is to perform topology optimization of a few basic problems in civil engineering applying Isogeometric analysis. The topology optimisation requires the sound knowledge of Isogeometric analysis. The literature review is done extensively and the existing work by several authors in the field of civil engineering is thoroughly reviewed [66]. The basic problems in Civil Engineering were solved and different types of problems were identified, and segregated.

As shown in the Fig.5 the approach model and formulation for each type of problem is performed first and then we applied the isogeometric concept to analyse the domain. The basis functions were derived using NURBS which define the geometry of the domain. The same basis functions were used to compute the displacements, and the co-ordinates at any point of the structure. For each problem, the degree of the NURBS and the knot vector are determined first and the mathematical formulation is done. The necessary governing equations were developed and a process to analyse as shown in the Fig. 6 is developed and the coding is done in MatLab® to solve the design domains.

The optimisation process flowchart connector (C) has been developed as shown in the Fig.7. The process parameters and variables have been identified. The process begins with the initial set of values for the variables. The parameters such as lower limit for the elemental stress at the centroid and the lower limit for the relative density of each element are set initially at the beginning of the flowchart. The material properties namely the Young's modulus of elasticity and the Poisson's ratio are taken as input. The initial values for the relative density variable of each element is generated. The process is repeated until the convergence criteria which is the number of iterations is reached. The graph showing the convergence of the objective function with the objective function on *Y*-axis and the number of iterations on *X*-axis are plotted.

3.1 Assumptions for plates carrying in the plane loading

1. The reinforced concrete section is assumed to be fully cracked section at ultimate state.
2. The principal stress is calculated at the centroid of each element and verified with the allowable principal stress for the given material.
3. The material is assumed to be homogeneous and Isotropic.

3.2 Problem statement
3.2.1 Plates carrying in plane loading

The aim of the project is to find an optimal linearly elastic structure with the help of isogeometric analysis which gives more accurate solutions compared to finite element analysis. Optimal solution refers to a design which is light but strong and rigid at the same time i.e mathematically our goal is to minimize the weight of the structure that is indirectly maximizing the total forces that are acting on the structure.

An objective function describes the main aim of the model whether to minimize or maximize the objective function and also our objective is to minimize the weight of the structure subject to constraints as well. Minimize, the compliance of the structure subjected to

$$\sigma_{\max\, principal} \le \sigma_{allowable}$$
$$u_{\max\, nodal} \le u_{allowable}$$
$$\left(\sum_{i=1}^{n} \rho_i v_i\right) * \bar{\rho} \succ 0$$

where, ρ_i is the density parameter of the element, v_i is the volume of the element, and $\bar{\rho}$ is the density of the material subjected to $V_a * v - \left(\sum_{i=1}^{n} \rho_i v_i\right) \ge 0$, where, V_a is the allowable material in percentage, and v is the volume of the structure $0 \le \rho_{\min} \le \rho_e \le 1$, where σ is stress constraint, u is displacement constraint, v is volume constraint and ρ is relative density with given state variables Young modulus 'E' and Poisson's ratio 'υ' along with Neumann and Dirichlet boundary conditions.

The objective is to find the minimum weight of the structure subjected to the constraint on the amount of material used and the elemental stresses and nodal displacements in the structure. The corresponding global stiffness matrix is given by

$$K = \sum_{e=1}^{N_e} \rho_e^p k_e$$

3.2.2 Laminated composite plates carrying out of plane loading

The plate is discretised with 24 × 24 elements. Each element in the control mesh has 16 control points. The degree of the polynomial is taken as equal to 3. C^2 connectivity is ensured. 16 point gauss quadrature is used to perform the numerical integration and form the stiffness matrix for each element. The NURBS polynomials and the derivatives are given in Appendix A.

A SSSS laminated composite plate having dimensions 1 × 1 is subjected to sinusoidal loading along both the directions. The ratio of the Young's modulus along two directions is taken as 25. The thickness of the laminate is equal to 0.01. The Poisson's ratio is equal to 0.25. The Shear modulus are related using the following relation and are given below [67].

$E_1/E_2 = 25$, $a = 1$; $b = 1$; $E_1 = 25 \times 10^3$; $E_2 = 1 \times 10^3$; thick = 0.01; $Nu = 0.25$; $G_{12} = 0.5 \times 10^3$;
$G_{13} = 0.5 \times 10^3$; $G_{23} = 0.2 \times 10^3$

The support boundary conditions for all the control points along the x-axis is taken as 101. The support boundary conditions for all the control point along the y-axis is taken as 011.

(a) Static analysis of SSSS laminated composite square plate.

The plate is discretised using 729 nodes with 24 × 24 elements. Each element in the control mesh has 16 control points. The degree of the NURBS polynomial is taken as equal to 3. There are three points overlapping between two elements. One node in common will ensure C^0 connectivity. Two nodes in common will ensure C^1 connectivity. Three nodes in common will ensure C^2 connectivity. 16 gauss point quadrature is used to perform the numerical integration and form the stiffness matrix for each element. The non-dimensional central displacement is compared with the analytical results given in the literature.

(b) Topology optimisation of SSSS laminated composite square plate using strain energy as the objective function. The plate is optimised for several different lamina and optimise $0.5 \times U^T \times K \times U$. The deflected shape of the optimised laminate is presented and discussed.

3.3 Research significance

Topology optimisation of reinforced concrete structures is an interesting and a complex domain of research. To determine the optimal layout of steel within the domain is an NP-Hard problem. When the domain is new and carries multiple loadings the task to determine the optimal layout of main steel is an uphill task. A few methods such as strut-and-tie method has been proposed in the past which are easy to handle when a single point concentrated load is acting on the structure. In case of multiple loadings, the strut-and-tie model has to be determined for each load applied individually and then determine the final form of layout of steel. This requires lot of time and effort. Topology optimisation can give a better solution when multiple loads are acting on the structure at the same time. Isogeometric analysis is a well proven method to analyse the structure as it accounts for an exact geometry and uses basis functions derived from the geometry of the structure. The nodal displacements, strains and stresses can be precisely calculated when compared with the traditional finite element analysis. The use of B-splines, NURBS and T-Splines can give us a precise geometrical description of the structure. In addition to this, a measure of the performance of the structure is required to determine the efficiency of the distribution of the material. Performance Index based on compliance of the structure can a suitable measure to assess the material distribution.

There is a need to use a precise method and give us an exact measure of the stresses developed and the energy carried by the structure. The main focus of this research study is to apply isogeometric analysis and perform topology optimisation of reinforced concrete domain to determine the optimal layout of the material. The stress distribution can give us more information on the areas where the tensile stresses are developed and sufficient reinforcement can be provided to carry these stresses. Throughout the analysis the concrete section is assumed as a fully cracked section within the elastic limit.

The present study on iso-geometric analysis for topology optimisation of laminated composites opens up a new door for research area in Civil Engineering. The advantages of applying iso-geometric analysis over finite element analysis is well known from the literature over the past decade. Laminated composites are being used in several areas of Engineering such as shell roofings, bridges, automobile, marines and aeronautical applications, for example components of rockets and aircrafts. The exactness and speed of precision of iso-geometric analysis is an advantage over other methods. There is a need to do further research in this area of laminated composites.

3.4 Flowchart

The flowchart for Integrated Topology optimization [65] is as shown below in Fig.5. Topology optimisation is the first step which shows the broad outline of the distribution of material. The design is then improved in CAD software by smoothing the boundaries. The model is then analysed using an software package Solid Works® and if successful it then finally optimised usign DesignWorks®. In case the analysis in Solid Works fails then the model is redesigned. This process continues until the analysis is done and the stresses and displacements are well within the permissible limits. The final design obtained is then casted for use.

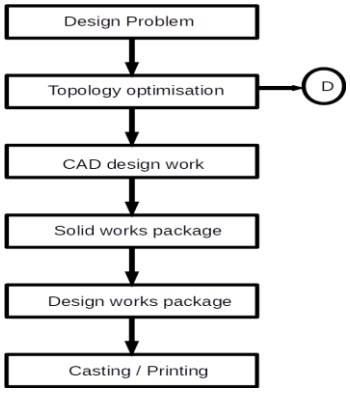

Fig.5
Integrated topology optimisation [64][65].

The design problem is the physical problem with the given constraints. Topology optimisation is performed to determine the optimal distribution of material within the given material domain subjected to the given constraints. The output is then import into CAD work and the design is smoothened by eliminating the corners. The material distribution is then analysed using Solid works® and Design works® packages as shown in the Fig.5. The final design is then either casted or 3D printed [65]. The entire process is iterative which means that the final distribution of material is arrived after several cycles. The focus of this study is to perform topology optimisation and does not deal with the other steps in the design process. Topology optimisation can give a broad idea of the layout of material. This step in the design process will show the direction for the layout of the material.

The literature review is performed and the rational type B-spline basis functions are formulated in this study. Static analysis is performed to verify the formulation. The code is written in MATLAB. Fig.5 shows the flowchart to perform topology optimisation. The program is divided into two modules.

(a) Static analysis module

(b) Topology optimisation module

The input data of the structure is divided into four areas namely

- The geometry
- The material property
- Force boundary conditions
- Displacement boundary conditions

The geometry data consists of length and breadth of the plate, the thickness of the plate. The material property consists of Modulus of elasticity E_{11} and E_{22}, shear modulus of elasticity G_{12}, G_{13}, G_{23} and the Poisson's ratio. The force boundary conditions comprise of the loading, which is sinusoidal loading. The displacement boundary conditions consist of the support conditions, in this case it is simply supported plate on all four sides. Fig.6 shows the steps involved to perform static analysis.

For in case of isotropic material, $E_{11} = E_{22} = E$

In case of isotropic material, $G_{12} = G_{23} = G_{13}$

The optimisation module consists of first order sensitivity analysis. The first derivative of the strain energy is used to perform sensitivity analysis. The optimality criteria is used to determine the relative densities of each element and calculate the objective function. With the newer values of the relative density the stiffness matrix is assembled again and the nodal displacements are determined. The process repeats until convergence is met. Same flow chart can be useful to perform topology optimisation for different lamina as shown in the Fig.7

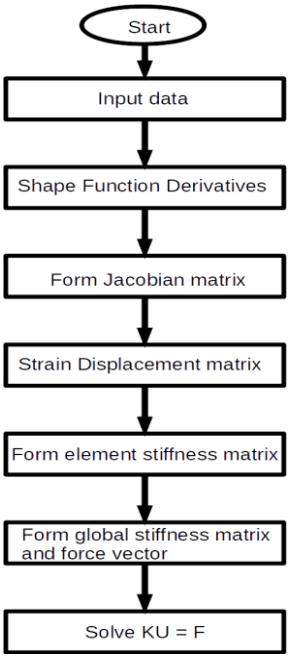

Fig.6
Flow chart for static analysis.

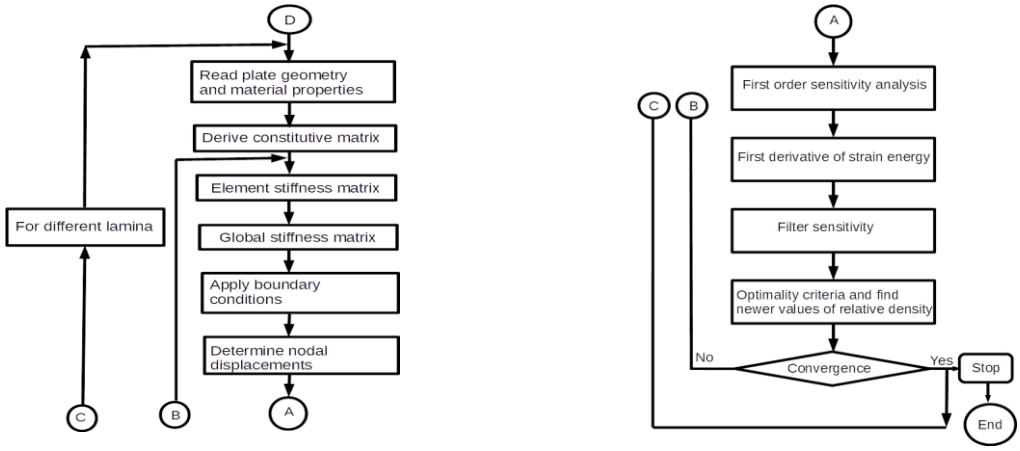

Fig.7
Flowchart for topology optimization.

4 ISOGEOMETRIC TOPOLOGY OPTIMISATION OF PLATES CARRYING IN PLANE LOADING

The numerical problems are modeled and analysed in this section using iso-geometric analysis. The reinforced concrete domain is modeled using B-splines with the degree along *x*-axis equal to one and *y*-axis equal to one. Topology optimisation of the RC structure is performed using Iso-geometric analysis with minimising the compliance as the objective function and optimality criteria as the optimizer to redistribute the relative density of the elements. Sensitivity analysis is performed to determine the newer values of the objective function with first order approximation by eliminating all the higher order terms in Taylor series. Few problems are solved here to determine the strut and tie models for each reinforced concrete section. The strut and tie models using the proposed method are compared with the strut and tie models in the literature and checked for validity of the proposed method. The performance index as given by Liang [68] is determined for each distribution for each iteration. The performance index is used as an indicator of the efficiency of the strain energy of the distribution, it is calculated by neglecting the higher order terms in the sensitivity analysis.

4.1 Simply supported beam with the left end hinge and right end roller carrying a point load at the centre acting vertically downwards

A initial design domain of MBB beam is as shown in the Fig. 8. The plate is having the dimensions of 600 *mm* length and 100 *mm* height and thickness of one unit. The plate is simply support with a hinge at the left end support and a roller support at the right end. A load of magnitude 100 *N* is applied acting vertically downwards at the centre node of the top edge. The domain is meshed using 120 × 20 first order four node quadrilateral elements. The dimensions of each element is 5 *mm* × 5 *mm*. The Young's modulus of Elasticity is taken as 200 *GPa* and the Poisson's ratio is taken as 0.30. The degree of polynomial for B-splines is taken as one along both the directions, p=1 and q=1. Iso-geometric analysis [69] is used to perform the static analysis and determine the displacements at each control point in each iteration. The optimisation is performed using Strain Energy as the objective function. Optimality criteria is used to determine the relative densities of each element during the optimisation.

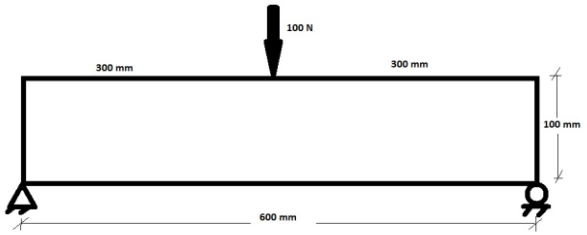

Fig.8
Hinge support on the left and roller support on the right.

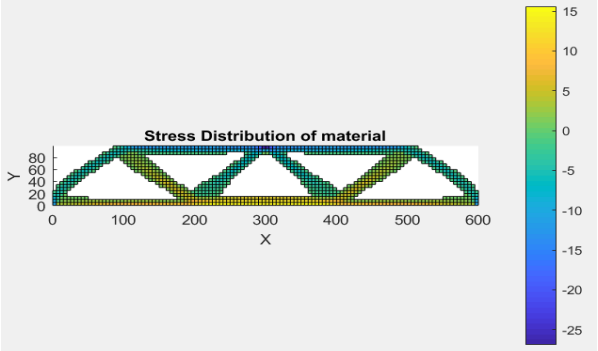

Fig.9
IGA Stress distribution of MBB Beam.

The optimal distribution of material for MBB beam using the present method is as shown in the Fig.9. The optimal distribution of material presented by Anna [70] is as shown in the Fig. 10. The stress distribution shows tha the maximum compressive stress in the material is indicated by blue region is about 25 *MPa*. The maximum tensile stress shown in yellow color is about 15 *MPa*. The distribution of material along the horizontal line joining the supports is carrying tensile stress indicating it is a tie member of the truss. The material on the top edge is in blue color carrying compressive stress is similar to a strut member of the truss. The inclined members in blue color are carrying compressive stress and the inclined members in yellow color are carrying tensile stress.

Fig.10
Distribution of material for MBB beam presented by Anna[70].

The penalisation factor for Youngs' Modulus of Elasticity is equal to 2 required to penalise the stiffness matrix. The total number of iterations required is 36. The move limit is taken as 0.30 and the stabilisation factor, SF is equal to 0.50. The final volume is equal to 0.30 and the filter radius is set equal to 2. The minimum stress cutoff to plot the stress distribution in the material is equal to 0.75.

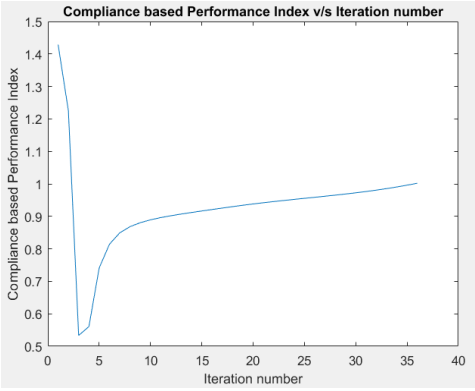

(a)

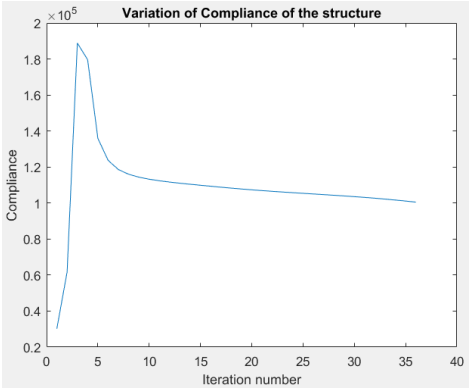

(b)

Fig.11
(a) Compliance based performance index. (b) Compliance of the structure.

Fig.11 showing the variation of compliance-based index and total compliance of the structure for each iteration. The variation of compliance-based performance index for each iteration is as shown in the Fig.11(a). The performance index at convergence is equal to 1.0. The variation of the compliance of the structure for each iteration is as shown in the Fig.11(b). The compliance of the structure at convergence is nearly equal to 1.0e5 *N-mm*.

4.1.1 Simply supported beam having both ends hinged carrying a point load acting vertically downwards at the centre of the top edge

A simply supported beam having both ends pinned is 600 *mm* length and 100 *mm* depth. The thickness of the beam is equal to unity. The beam is supported on hinge supports at both the lower ends. A point load of 100 *N* is acting vertically downwards at the centre of the beam on the top edge as shown in the Fig.12. The domain is composed using 120 × 20 first order four node quadrilateral elements. The dimensions of each element is 5 *mm* × 5 *mm*. The Young's modulus of Elasticity is taken as 200 *GPa* and the Poisson's ratio is taken as 0.30. The optimisation is performed using Strain Energy as the objective function. Optimality criteria is used to determine the relative densities of each element during the optimisation.

The penalisation factor for stiffness is taken as equal to 2. The filter radius is 2 and the stabilitsation factor is taken as 0.50. The move limit is 0.10. The total number of iterations required are 36. The final volume fraction is equal to 0.3. Stabilisation factor is equal to 0.5 and the cutoff relative density for display is 0.2. The minimum Stress is equal to 0.50.

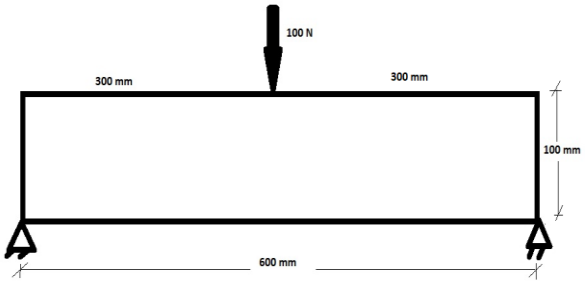

Fig.12
Shows the initial domain.

Fig.13
Shows the optimal distribution of material by Anna [70].

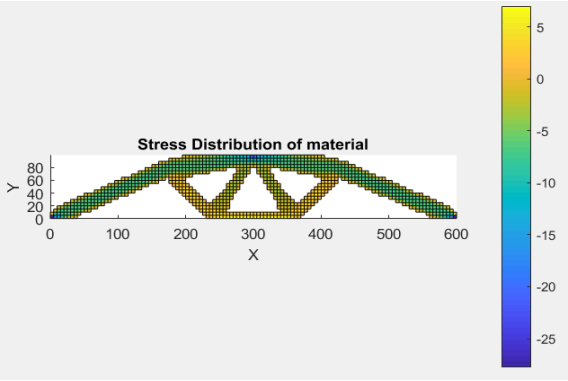

Fig.14
IGA stress distribution of the beam at optimal state.

The stress distribution of the beam hinged at both the ends using the present method is as shown in the Fig.14. The distribution of material is given by Anna as shown in the Fig. 13. The stress distribution is similar to a strut and tie model showing tensile and compressive stress over the design domain. The green color to blue color indicates elements carrying compressive stress. The maximum compressive stress is equal to 25 *MPa*. The orange color to yellow color indicates elements carrying tensile stress. The maximum tensile stress is about 5 *MPa*. Fig.15(a) Shows the variation of the performance index for each iteration. The maximum value of performance index at convergence is equal to 1.50. Fig.15(b) Shows the variation of the total compliance of the structure on *Y*-axis with each iteration on *X*-axis. The total compliance of the structure at convergence is equal to 3e4 *N-mm*.

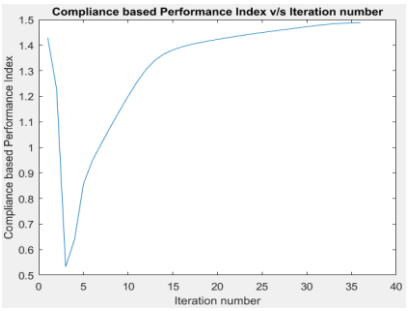

(a)

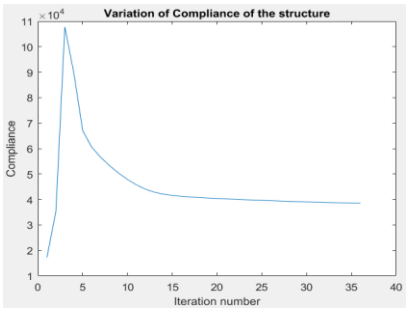

(b)

Fig.15
(a) Compliance based performance index. (b) Compliance of the structure.

Fig.15 showing the variation of (a) the compliance based performance index and (b) total compliance of the structure with iteration number.

4.2 Simply supported plate with both ends supports as hinged and carrying point load at the centre of the bottom edge - Michelle truss

A simply support plate has both the ends as hinged carries a point load of magnitude 10 N acting vertically downwards at the centre of the bottom edge as shown in the Fig.16. The dimensions of the plate are $2H \times H$, where $2H$ is the length parallel to horizontal axis and H as the vertical depth. The side H is taken as equal to 160 mm. The Young's modulus of elasticity of the material is taken as 200 GPa and the Poisson's ratio is equal to 0.30. The control mesh of domain is taken as 64×32 four node quadrilaterals. The size of each quadrilateral is $5\ mm \times 5\ mm$ square. The total number of nodes is equal to 2145 and total number of quadrilateral elements is 2048. The thickness of the plate is taken as equal to 1 mm.

The total number of iterations is equal to 66. The penalisation factor for stiffness is taken as equal to 2, and filter radius is equal to 2. The move limit is equal to 0.05. The cut off for display of relative density is equal to 0.1. The minimum stress for display is taken as equal to 0.01. The distribution of material within the domain is as shown in the Fig.16(b). The stress distribution for the optimal distribution is as shown in the Fig.16(b). The maximum stress is equal to 1 MPa in tension and compression.

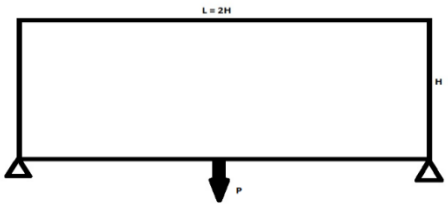

(a)

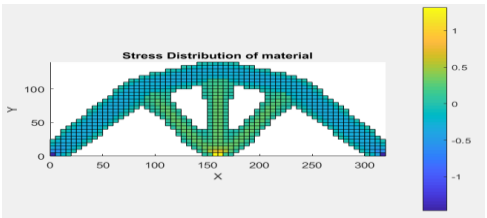

(b)

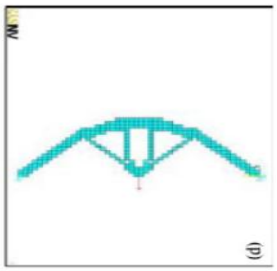

(c)

Fig.16
(a) Initial design domain. (b) IGA Stress distribution at optimal state. (c) optimal distribution by Abolbashari [71].

Fig.16 shows initial design domain and optimal distribution of material for supported plate having both the supports as hinged (Michelle Truss). The initial design domain is as shown in Fig. 16(a). The optimal distribution as shown in Fig.16(b) clearly shows the regions where the elements are carrying tensile stress indicated in green color

and yellow color. The maximum value of the tensile stress is about 1*MPa*. The region in blue color are elements carrying compressive stress. The maximum value of the compressive stress is about 1 *MPa*. Fig.16(c) shows the optimal distribution of material presented by Abolbashari [71].

The variation of compliance for each iteration is as shown in Fig.17(a). The compliance-based performance index for each iteration is as shown in the Fig.17(b). The maximum performance index at convergence is equal to 1.0. The compliance of the structure at convergence is equal to 50 *N-mm.*

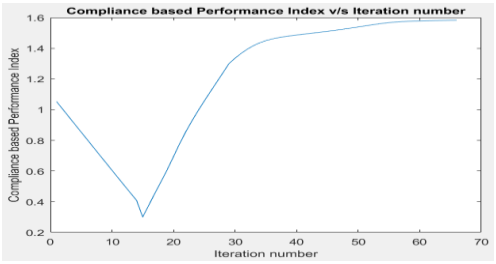

(a)

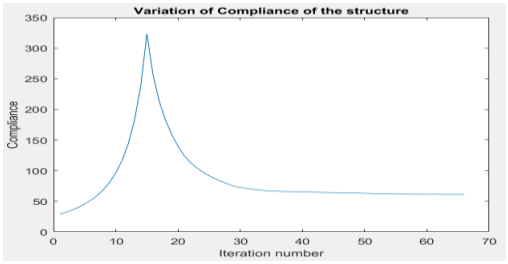

(b)

Fig.17
(a) Performance Index. (b) Compliance of the structure.

Fig.17 Variation of the performance index and the total compliance of the structure.

4.2.1 Simply supported plate having left end hinged and right end roller support carrying a point load acting vertically downwards at the centre of the line joining the supports

A simply supported plate with the left end hinged and right roller is having the dimension of $2H \times H$, where $2H$ is the length parallel to the horizontal axis and H is the depth in the vertical direction as shown in the Fig.18. The thickness of the plate is one unit. The side H is equal to 160. The plate carries a point load of magnitude $10N$ acting vertically downwards at the centre of the bottom edge of the plate joining the supports. The total number of control points is equal to 2145 and the total quadrilaterals is equal to 2048. The control mesh of the domain is 65×33. The Young's modulus of elasticity of the material is equal to 200 *GPa* and the Poisson's ratio is equal to 0.30.

The total number of iterations required is equal to 80. The penalisation factor for stiffness matrix is equal to 2 and the move limit is taken as 0.05. The fraction volume of the domain is equal to 0.3. The stabilisation factor is equal to 0.5. The minimum stress for cutoff is taken as equal to 0.01. The stress distribution of the material is as shown in the Fig.18(b). Fig.18(c) shows the distribution of material presented by Abolbashari [71]. The distribution of material obtained using the present method IGA is similar to the distribution given in the literature.

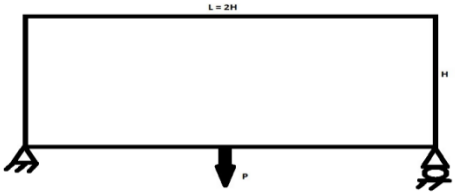

(a)

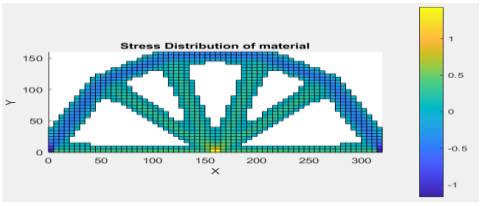

(b)

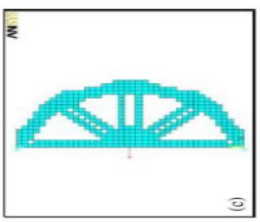

(c)

Fig.18
(a) Initial design domain.(b) Optimal distribution using IGA.
(c) Optimal distribution of material by Abolbashari [71].

Fig.18 shows the initial domain and the optimal distribution of material. The variation of the compliance of the structure is as shown in the Fig.19. The initial portion of the curve is rising which is due to a term change in

compliance (dC) included in the optimality criteria. The results are valid at convergence. Fig.19 shows the variation of the compliance-based performance index on *Y*-axis and for each iteration on *X*-axis. The performance index is observed to be reducing during the initial portion of the curve and this is due to the similar reason said above. The values of the performance index are valid at convergence. The elements in blue color indicates compressive stress. The maximum value of the compressive stress is equal to 1 *MPa*. The elements in green color and yellow color indicates the elements are carrying tensile stress. The maximum value of the tensile stress for this fan like optimal distribution of material is about 1 *MPa*.

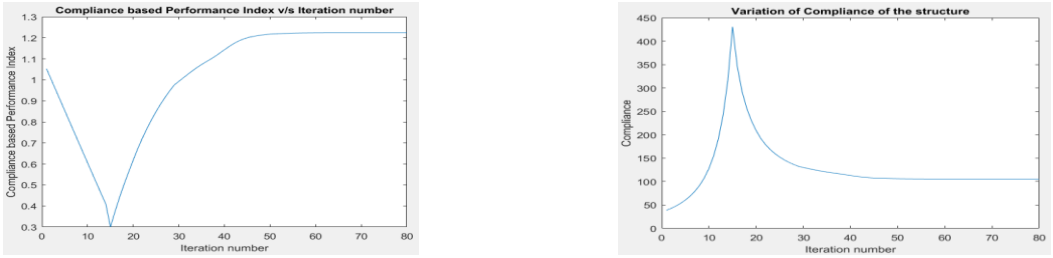

(a) (b)

Fig.19
(a) Compliance based Performance Index. (b) Compliance of structure.

Fig.19 Variation of (a) Compliance based performance index and (b) Compliance of the structure with iteration number

4.3 Bridge design

A rectangular plate area of 5000 *mm* × 2500 *mm* is hinged on both corners at the bottom edge. The plate is divided into 1250 quadrilaterals and 1326 control points. The size of each quadrilateral is 100 *mm* × 100 *mm*. The Youngs' modulus of elasticity of the plate is 20 *GPa* and the Poisson's ratio is taken as 0.10. The thickness of the plate is one unit. The plate carries a uniformly distributed load of 20 N/m. Two types of loading acting on the bridge are considered as follows:

(a) Through type bridge design in which udl is applied at the bottom edge over the entire span of 5000 *mm* between the supports.
(b) Deck type bridge design in which udl is applied at the top edge over a length of 5000 *mm*.

For stiffness matrix, the penalisation factor for Youngs' modulus of elasticity is equal to 4. The filter radius is taken as two and the move limit is equal 0.05. The stabilisation factor is taken as 0.50 and the fraction volume is equal to 0.30. The number of iterations required for convergence is equal to 50. The cutoff for minimum stress is taken as equal to 0.12 for display for the deck type bridge. The stress in the optimal distribution of material is compressive in nature as shown in the Fig.20. The maximum compressive stress is about 6 *MPa*. For the through type bridge design, the minimum stress intensity for cutoff is taken as 1e-3 to display the optimal distribution of material. The maximum compressive stress is 6 *MPa* and the tensile stress is nearly 1 *MPa*. The arch in green color shows that compressive stresses are developed. The distribution of material as given by *XY* Yang is as shown in the Fig.21. The distribution of material using the proposed method using iso-geometric analysis is similar to the distribution of material given in the literature.

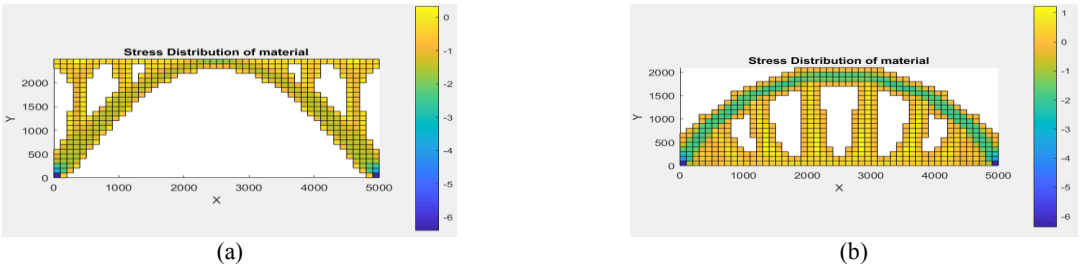

(a) (b)

Fig.20
(a)Deck type bridge design. (b) Through type design.

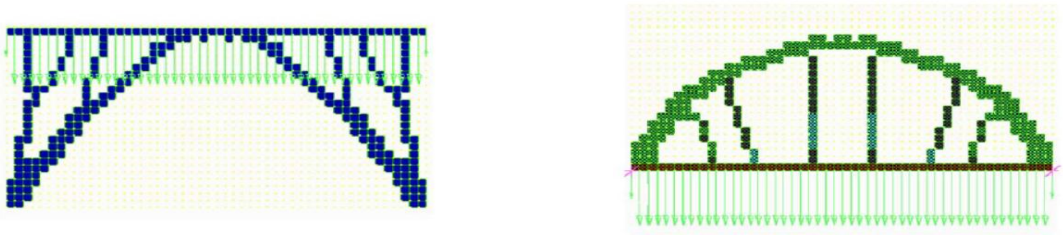

(a) (b)

Fig.21
Distribution of material given by *X Y* Yang [72].

5 STATIC ANALYSIS OF LAMINATED COMPOSITE SQUARE PLATE USING ISOGEOMETRIC ANALYSIS

The static analysis of the SSSS laminated composite plate is performed here. The mesh is 24 × 24 elements and the total number of control points are 27 × 27 = 729.

The problem statement is given in section 3.2.2 and the step-by-step procedure to determine the second derivatives using six elements is given in great detail in Appendix A. The Input data is given as follows.

$E_1/E_2 = 25$, $a = 1$; $b = 1$; $E_1 = 25 \times 10^3$; $E_2 = 1 \times 10^3$; thick = 0.01; $Nu = 0.25$; $G_{12} = 0.5 \times 10^3$; $G_{13} = 0.5 \times 10^3$; $G_{23} = 0.2 \times 10^3$

$$\text{Xi Knot vector} = \left\{ 0 \;\; 0 \;\; 0 \;\; 0 \;\; \frac{1}{24} \;\; \frac{2}{24} \;\; \frac{3}{24} \;\; \frac{4}{24} \;\; \frac{5}{24} \;\; \frac{6}{24} \;\; \frac{7}{24} \;\; \frac{8}{24} \;\; \frac{9}{24} \;\; \frac{10}{24} \;\; \frac{11}{24} \;\; \frac{12}{24} \;\; \frac{13}{24} \;\; \frac{14}{24} \;\; \frac{15}{24} \;\; \frac{16}{24} \;\; \frac{17}{24} \;\; \frac{18}{24} \;\; \frac{19}{24} \;\; \frac{20}{24} \;\; \frac{21}{24} \;\; \frac{22}{24} \;\; \frac{23}{24} \;\; \frac{24}{24} \;\; \frac{24}{24} \;\; \frac{24}{24} \;\; \frac{24}{24} \right\}$$

$$\text{Eta Knot vector} = \left\{ 0 \;\; 0 \;\; 0 \;\; 0 \;\; \frac{1}{24} \;\; \frac{2}{24} \;\; \frac{3}{24} \;\; \frac{4}{24} \;\; \frac{5}{24} \;\; \frac{6}{24} \;\; \frac{7}{24} \;\; \frac{8}{24} \;\; \frac{9}{24} \;\; \frac{10}{24} \;\; \frac{11}{24} \;\; \frac{12}{24} \;\; \frac{13}{24} \;\; \frac{14}{24} \;\; \frac{15}{24} \;\; \frac{16}{24} \;\; \frac{17}{24} \;\; \frac{18}{24} \;\; \frac{19}{24} \;\; \frac{20}{24} \;\; \frac{21}{24} \;\; \frac{22}{24} \;\; \frac{23}{24} \;\; \frac{24}{24} \;\; \frac{24}{24} \;\; \frac{24}{24} \;\; \frac{24}{24} \right\}$$

$$\text{Control points along } X\text{-axis} = \left\{ 0 \;\; \frac{1}{72} \;\; \frac{1}{24} \;\; \frac{2}{24} \;\; \frac{3}{24} \;\; \frac{4}{24} \;\; \frac{5}{24} \;\; \frac{6}{24} \;\; \frac{7}{24} \;\; \frac{8}{24} \;\; \frac{9}{24} \;\; \frac{10}{24} \;\; \frac{11}{24} \;\; \frac{12}{24} \;\; \frac{13}{24} \;\; \frac{14}{24} \;\; \frac{15}{24} \;\; \frac{16}{24} \;\; \frac{17}{24} \;\; \frac{18}{24} \;\; \frac{19}{24} \;\; \frac{20}{24} \;\; \frac{21}{24} \;\; \frac{22}{24} \;\; \frac{23}{24} \;\; \frac{71}{72} \;\; \frac{24}{24} \right\}$$

$$\text{Control points along } Y\text{-axis} = \left\{ 0 \;\; \frac{1}{72} \;\; \frac{1}{24} \;\; \frac{2}{24} \;\; \frac{3}{24} \;\; \frac{4}{24} \;\; \frac{5}{24} \;\; \frac{6}{24} \;\; \frac{7}{24} \;\; \frac{8}{24} \;\; \frac{9}{24} \;\; \frac{10}{24} \;\; \frac{11}{24} \;\; \frac{12}{24} \;\; \frac{13}{24} \;\; \frac{14}{24} \;\; \frac{15}{24} \;\; \frac{16}{24} \;\; \frac{17}{24} \;\; \frac{18}{24} \;\; \frac{19}{24} \;\; \frac{20}{24} \;\; \frac{21}{24} \;\; \frac{22}{24} \;\; \frac{23}{24} \;\; \frac{71}{72} \;\; \frac{24}{24} \right\}$$

Table 3
Non-dimensional deflection at centre of SSSS plate subjected to sinusoidal loading.

Lamina/mesh	12 × 12	24 × 24	Theoretical	Ratio
0/90/0	0.4482	0.4357	0.4343 [73, Table 2],[67, Table 1]	1.003
0/90	1.1040	1.0743	1.0742 [73, Table 6]	1.000
0/90/90/0	0.4478	0.4356	0.4347 [62, Table 3]	1.002

The results obtained using 24 × 24 elements as shown in the Table 3 are nearly equal to the analytical results given in the literature. We can perform topology optimisation in the next section.

5.1 SSSS plate having Angle ply lamina θ/-θ/θ/-θ subjected to sinusoidal loading

$E_1/E_2 = 25$, $a = 1$; $b = 1$; $E_1 = 25 \times 10^3$; $E_2 = 1 \times 10^3$; thick = 0.01; $Nu = 0.25$; $G_{12} = 0.5 \times 10^3$; $G_{13} = 0.5 \times 10^3$; $G_{23} = 0.2 \times 10^3$

Table 4
Non-dimensional deflection for SSSS plate carrying sinusoidal loading with varying fibre orientation.

Lamina	0/0/0/0	15/-15/15/-15	30/-30/30/-30	45/-45/45/-45
Non-dimensional	0.4357	0.3892	0.3001	0.2665
Lamina	60/-60/60/-60	75/-75/75/-75	90/-90/90/-90	
Non-dimensional	0.3002	0.3894	0.4357	

The results in the Table 4 clearly show a symmetrical vertical non-dimensional displacements at the centre of the square plate carrying sinusoidal loading for different fibre angle orientation varying from 0 - 90.

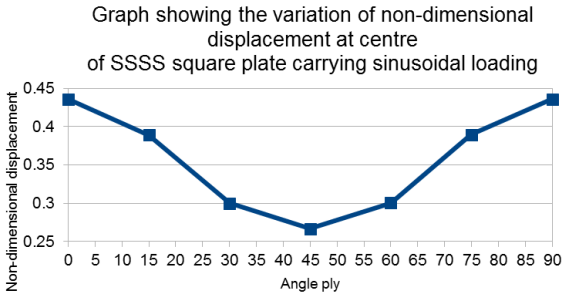

Fig.22
Variation of non-dimensional displacement at the centre of SSSS square plate for $\theta/-\theta/\theta/-\theta$.

The graph clearly shows that the non-dimensional vertical displacement is minimum when the fibre orientation is 45/-45/45/-45 as shown in the Fig.22. The graph is showing symmetrical non-dimensional deflection at the centre of the plate carrying sinusoidal loading for different values of fibre orientation varying from 0 - 90 degrees.

6 ISOGEOMETRIC TOPOLOGY OPTIMISATION OF LAMINATED COMPOSITE SQUARE PLATE SUBJECTED TO SINUSOIDAL LOADING

In the previous section, we have performed static analysis of SSSS laminated composite plate. The applied mechanical load is sinusoidal load in both directions. In this section, we perform the topology optimisation of laminated composite plate using first order sensitivity analysis and optimality criteria for different lamina. The mesh is 24 × 24 elements with 729 nodes. The support boundary conditions for all control points along *x*- axis is 101 and the control points along the *y*-axis is 011 for displacement along *x, y, z* axes respectively. There is no rotation degree of freedom at any node.

The following input data is considered in this study. The penalisation factor is taken as equal to 2. The filter radius is equal to 2. The move limit is taken as 0.30 and the stabilisation factor is equal to 0.50. The final fraction of volume is taken as equal to 0.2.

6.1 SSSS plate having 0/90 lamina subjected to sinusoidal loading

The lamina considered for this problem is 0/90. The objective function is taken as strain energy of the structure. First order sensitivity analysis is performed and the relative densities are filtered. The optimality criteria is used to determine the newer values of the relative densities of each element and compute the objective function. The total number of iterations are 17. The deformed shape is as shown in the Fig.23. The elements at the centre of the edge are carrying higher values of relative density. These elements form an arrangement of a plus sign. The deflected

shape of the laminate shows that the sagging portion of the laminate appears to behave like a cloth. The magnitude of the load is kept constant and the relative densities are changed after each iteration. The portion of the material near the supports shows a large drop indicating that there is no bending moment. The deformed shape shows a pattern of U-shaped tub. The vertical displacement along the centre line is nearly equal in both the directions.

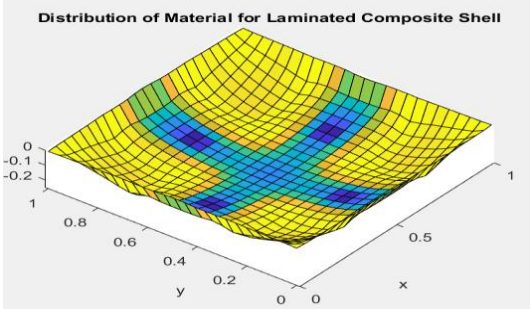

Fig.23
Isogeometric topology optimisation of SSSS plate having 0/90 lamina subjected to sinusoidal loading in 17 iterations.

6.2 SSSS plate having 0/90/90/0 lamina carrying sinusoidal loading

The SSSS plate having 0/90/90/0 symmetric lamina carries sinusoidal loading and optimised with strain energy as the objective function and optimality criteria is the optimsation method. The deformed profile after 16 iterations is as shown in the Fig.24. The distribution as shown in Fig.24(a) clearly shows the fibres along the *x*-direction near the centre of the plate are carrying higher value of strain energy. The deformed profile shows that the fibres on either sides of the centre line along the *x*-axis are sagging as shown in Fig.24(b).

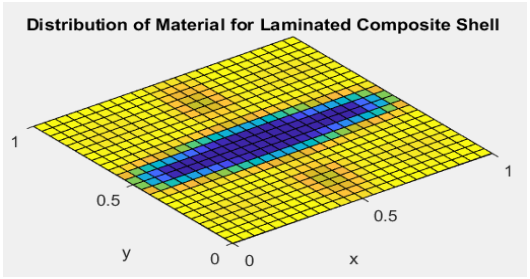

(a)

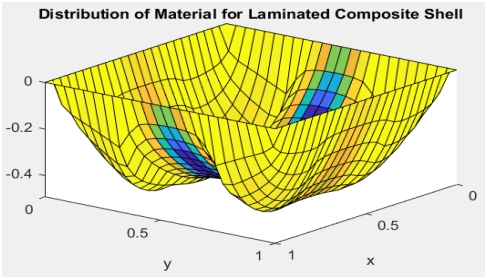

(b)

Fig.24
(a) Distribution of material at iteration16. (b) Deflected shape in three dimensions.

Fig.24 Iso-geometric topology optimisation of laminated composite plate having 0/90/90/0 lamina subjected to sinusoidal loading in 16 iterations.

6.3 SSSS plate having 0/90/0/90 lamina carrying sinusoidal loading

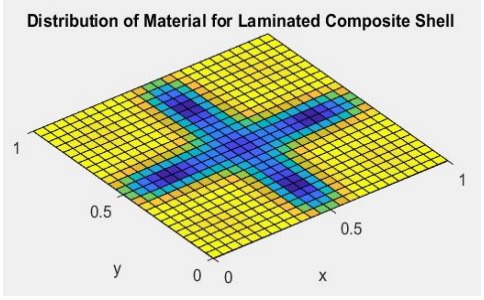

(a)Top view

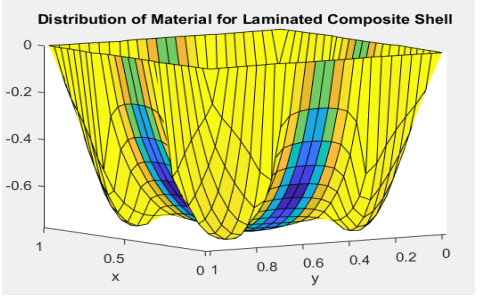

(b) Deformed profile

Fig.25
Iso-geometric topology optimisation of SSSS laminated composite plate having 0/90/0/90 lamina subjected to sinusoidal loading in 14 iterations.

The SSSS square plate having 0/90/0/90 lamina is anti-symmetric laminate carrying sinusoidal loading. The distribution of strain energy after optimisation using optimality criteria is as shown in the Fig.25. The elements along the centre line in the form of a plus sign carry higher value of strain energy. The deformed profile after 14 iterations of the laminate is as shown in Fig.25. The deformed profile is symmetrical about both the axis. The fibres near the corners are sagging more than the fibres near the centre of the plate. The deformed profile appears to behave like a cloth when the loading is applied even after few elements are penalised.

6.4 SSSS plate having lamina 45/-45/45/-45 subjected to sinusoidal loading

SSSS square plate having 45/-45/45/-45 lamina is subjected to sinusoidal loading is optimised with strain energy as the objective function and optimality criteria. The deformed profile is as shown in the Fig.26.

The following observations were made after every iteration during the optimisation process:

1. The yellow color in the inclined direction, joining the middle points of the edges, fibres along the 45 degrees angle are stretched.
2. The yellow color ring formation, and the stress distribution is uniform.
3. The width of yellow color ring has increased, the load is shared by neighbouring elements, stress distribution is equal in the vicinity of the element.
4. The yellow color is throughout the plate, stress distribution is nearly equal throughout the plate within the ring. The yellow color fading along inclined lines, the fibres along the 45 degrees are not carrying load. 5. Moving towards centre aligning themselves in the orientation of 0/90.
5. The top view in Fig.26(a) clearly shows the elements along the line joining the mid points of the adjacent edges are showing similar color indicating similar relative density value of each element. When the deflections are similar, the elasticity matrix and the strain displacement matrix are same, then the stress vector is also same.
6. The laminate forms a flat surface having higher value of vertical deflection within the ring form a tub as shown in Fig. 26(b).

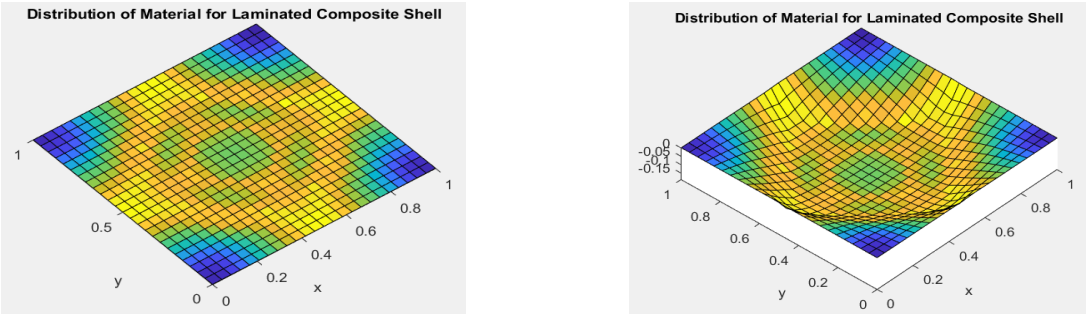

(a) Top view (b) Deformed profile

Fig.26
Isogeometric topology optimisation of SSSS square plate having 45/-45/45/-45 lamina in 15 iterations.

7 CONCLUSIONS

The current research topic on iso-geometric topology optimisation of steel, concrete and laminated composite plates and opens up a new door in the field of structural optimisation. The accuracy of iso-geometrical analysis over finite element analysis is well known from the literature over the past few years. In this study, three two-dimensional planar section problems are designed using topology optimisation. The objective function is to minimise the total compliance of the structure. First order sensitivity analysis is performed and optimality criteria is used to recalculate the relative densities of the elements. First problem, the problem of MBB beam is analysed using iso-geometric analysis. The total number of control points are 2541. The total number of iterations required are 36. The total compliance of the structure at convergence is equal to 1e5 *N-mm*. The performance index based on compliance is found to be 1.0 at convergence. The distribution of material obtained using isogeometric analysis is very similar to the distribution of material using finite element analysis. Second problem analysed is the Michelle truss problem. The total number of control points are 2145. The total number of iterations required are 66. The total compliance of

the structure is equal to 50 *N-mm* at convergence. The performance index is found to be 1.0. Third problem is the well known design of bridge problem from the given continuum material. Two types of loading were applied and the distribution of material for a deck type bridge and a through type bridge design are presented. A simply supported SSSS square laminate having different lamina is considered. The objective function is strain energy and optimality criteria is used as the optimisation method in this study. Four different problems have been solved with different lamina namely 0/90, 0/90/0/90, 0/90/90/0, 45/-45/45/-45. The formulation is done using the Kirchoff thin plate theory without any shear contribution. The governing equations are derived and given in the theoretical background section. The analysis is presented in three different section. The laminate having one unit dimensions is considered with the side to thickness ratio as 100. The ratio of the Young's modulus of elasticity is taken as 25 and the Poisson's ratio is equal to 0.25. The input data is chosen from the literature along with the analytical solution. The step-by-step procedure to determine the second derivatives is presented in section 4. The basis functions are derived for a cubic order spline polynomial. The derivation for the second derivative is given in detail. In the next section, the static analysis is performed to verify the maximum displacement at the centre of the plate carrying sinusoidal loading. The results from the Iso-geometric analysis are checked with the analytical results given in the literature. The plate having the lamina of 0/90, the maximum central non-dimensional deflection is found as 1.0743 compared with the analytical result of 1.0742. The plate having lamina of 0/90/0 has the maximum central non-dimensional deflection of 0.4357 and compared with the analytical solution is 0.4343. Another case of the plate having the 0/90/90/0 lamina, the maximum central non-dimensional deflection using iso-geometric analysis is found to be 0.4356 and the analytical solution is 0.4347. The results of static analysis using Iso-geometric analysis are in close agreement with those of the analytical solutions. The variation of non-dimensional vertical displacements were determined for θ /-θ /θ /-θ lamina varying the fibre orientation from 0 - 90 degrees is found to be symmetrical. The non-dimensional displacement is minimum when the fibre angle is 45 degrees.

Topology optimisation is performed in the next section. A square plate simply supported on all four sides having different lamina is optimised using optimality criteria with strain energy as the objective function. The lamina considered are 0/90, 0/90/0/90, 0/90/90/0, 45/-45/45/-45. The distribution of strain energy and the deformed profile are presented for each lamina. The deformed profile of the plate having 0/90 lamina is a trough with the elements along the centre line joining the mid points of the sides carry maximum value of strain energy. These elements form a plus sign. The deformed profile of the plate having 0/90/0/90 lamina is symmetric about the centre lines joining the midpoint of the edges. The elements near the corners were found to be sagging more than the element at the centre. For the case of the plate having 0/90/90/0 lamina, the strain energy distribution is found to be higher for all the elements along the centre line parallel to the *x*-axis. The elements adjacent to these are found to be sagging on either side of the centre along the *x*-axis. The plate having 45/-45/45/-45 lamina shows a symmetrical distribution of strain energy. The elements joining the lines joining the centre of the side s of the square carry higher value of strain energy. The portion of the laminate within these lines form a trough with a flat surface with equal vertical displacement.

APPENDIX

A step-by-step analysis of SSSS laminated composite plate subjected to sinusoidal loading. In the previous section, the necessary theoretical background and the governing equations are given. In this section, a square plate having 1 × 1 dimension is considered. The plate is simply supported and subjected to a sinusoidal loading in the both the directions. We perform a step by step formulation and the numerical answers required to compute second derivatives are given in this section. The stiffness matrix can be assembled using the governing equations. The Fig.5 shows the control mesh and the element wise nodes.

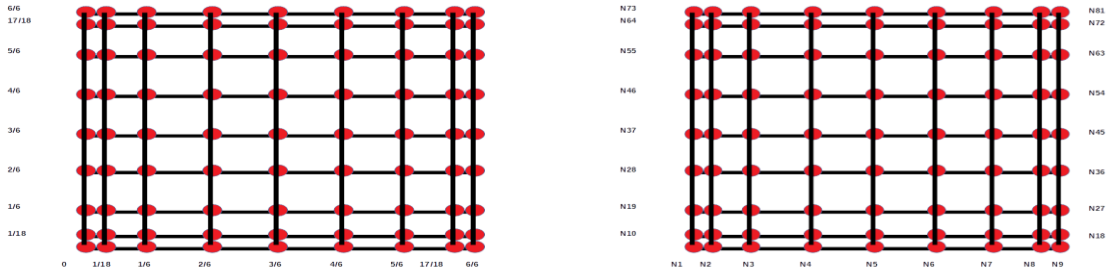

(a) Control points (b) Control mesh

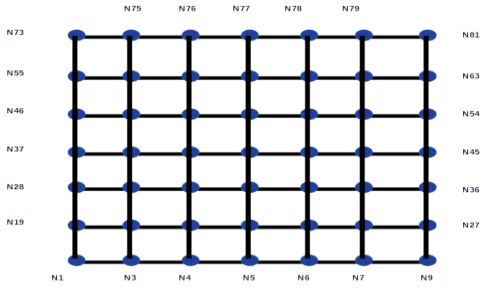

(c) Element wise nodes

SSSS laminated composite plate.

Table 1
Showing the control mesh for elements in the first two rows.

	N1	N2	N3	N4	N5	N6	N7	N8	N9	N10	N11	N12	N13	N14	N15	N16
1	1	2	3	4	10	11	12	13	19	20	21	22	28	29	30	31
2	2	3	4	5	11	12	13	14	20	21	22	23	29	30	31	32
3	3	4	5	6	12	13	14	15	21	22	23	24	30	31	32	33
4	4	5	6	7	13	14	15	16	22	23	24	25	31	32	33	34
5	5	6	7	8	14	15	16	17	23	24	25	26	32	33	34	35
6	6	7	8	9	15	16	17	18	24	25	26	27	33	34	35	36
7	10	11	12	13	19	20	21	22	28	29	30	31	37	38	39	40
8	11	12	13	14	20	21	22	23	29	30	31	32	38	39	40	41
9	12	13	14	15	21	22	23	24	30	31	32	33	39	40	41	42
10	13	14	15	16	22	23	24	25	31	32	33	34	40	41	42	43
11	14	15	16	17	23	24	25	26	32	33	34	35	41	42	43	44
12	15	16	17	18	24	25	26	27	33	34	35	36	42	43	44	45

Table 2
Showing the knot mesh for each element in the first two rows.

	1	2	3	4
1	1	3	21	19
2	3	4	22	21
3	4	5	23	22
4	5	6	24	23
5	6	7	25	24
6	7	9	27	25
7	19	21	30	28
8	21	22	31	30
9	22	23	32	31
10	23	24	33	32
11	24	25	34	33
12	25	27	36	34

$$N_{i,0} = \begin{cases} 1 & \xi_i \le \xi < \xi_{i+1} \\ 0 & otherwise \end{cases}$$

ξ_0	ξ_1	ξ_2	ξ_3	ξ_4	ξ_5	ξ_6	ξ_7	ξ_8	ξ_9	ξ_{10}	ξ_{11}	ξ_{12}
0	0	0	0	1/6	2/6	3/6	4/6	5/6	1	1	1	1

Table 3
Showing the basis functions.

	$N_{i,p}=\frac{\xi-\xi_i}{\xi_{i+p}-\xi_i}N_{i,p-1}+\frac{\xi_{i+p+1}-\xi}{\xi_{i+p+1}-\xi_{i+1}}N_{i+1,p-1}$	$\xi=\xi_3$	$\xi=\xi_4$	$\xi=\xi_5$	$\xi=\xi_6$	$\xi=\xi_7$	$\xi=\xi_8$
I=2, p=1	$N_{2,1}=\frac{\xi-\xi_2}{\xi_3-\xi_2}N_{2,0}+\frac{\xi_4-\xi}{\xi_4-\xi_3}N_{3,0}$	$(1-6\xi)N_{3,0}$	0				
I=3, p=1	$N_{3,1}=\frac{\xi-\xi_3}{\xi_4-\xi_3}N_{3,0}+\frac{\xi_5-\xi}{\xi_5-\xi_4}N_{4,0}$	$6\xi N_{3,0}$	$(2-6\xi)N_{4,0}$				
I=4, p=1	$N_{4,1}=\frac{\xi-\xi_4}{\xi_5-\xi_4}N_{4,0}+\frac{\xi_6-\xi}{\xi_6-\xi_5}N_{5,0}$		$(6\xi-1)N_{4,0}$	$(3-6\xi)N_{5,0}$			
I=5, p=1	$N_{5,1}=\frac{\xi-\xi_5}{\xi_6-\xi_5}N_{5,0}+\frac{\xi_7-\xi}{\xi_7-\xi_6}N_{6,0}$			$(6\xi-2)N_{5,0}$	$(4-6\xi)N_{6,0}$		
I=6, p=1	$N_{6,1}=\frac{\xi-\xi_6}{\xi_7-\xi_6}N_{6,0}+\frac{\xi_8-\xi}{\xi_8-\xi_7}N_{7,0}$				$(6\xi-3)N_{6,0}$	$(5-6\xi)N_{7,0}$	
I=7, p=1	$N_{7,1}=\frac{\xi-\xi_7}{\xi_8-\xi_7}N_{7,0}+\frac{\xi_9-\xi}{\xi_9-\xi_8}N_{8,0}$					$(6\xi-4)N_{7,0}$	$(6-6\xi)N_{8,0}$
I=8, p=1	$N_{8,1}=\frac{\xi-\xi_8}{\xi_9-\xi_8}N_{8,0}+\frac{\xi_{10}-\xi}{\xi_{10}-\xi_9}N_{9,0}$						$(6\xi-5)N_{8,0}$
I=1, p=2	$N_{1,2}=\frac{\xi-\xi_1}{\xi_3-\xi_1}N_{1,1}+\frac{\xi_4-\xi}{\xi_4-\xi_2}N_{2,1}$	$(1-6\xi)N_{2,1}$					
I=2, p=2	$N_{2,2}=\frac{\xi-\xi_2}{\xi_4-\xi_2}N_{2,1}+\frac{\xi_5-\xi}{\xi_5-\xi_3}N_{3,1}$	$6\xi N_{2,1}+\frac{(2-6\xi)}{2}N_{3,1}$	$\frac{(2-6\xi)}{2}N_{3,1}$				
I=3, p=2	$N_{3,2}=\frac{\xi-\xi_3}{\xi_5-\xi_3}N_{3,1}+\frac{\xi_6-\xi}{\xi_6-\xi_4}N_{4,1}$	$\frac{6\xi}{2}N_{3,1}$	$\frac{6\xi}{2}N_{3,1}+\frac{3-6\xi}{2}N_{4,1}$	$\frac{3-6\xi}{2}N_{4,1}$			
I=4, p=2	$N_{4,2}=\frac{\xi-\xi_4}{\xi_6-\xi_4}N_{4,1}+\frac{\xi_7-\xi}{\xi_7-\xi_5}N_{5,1}$	0	$\frac{6\xi-1}{2}N_{4,1}$	$\frac{6\xi-1}{2}N_{4,1}+\frac{4-6\xi}{2}N_{5,1}$	$\frac{4-6\xi}{2}N_{5,1}$		
I=5, p=2	$N_{5,2}=\frac{\xi-\xi_5}{\xi_7-\xi_5}N_{5,1}+\frac{\xi_8-\xi}{\xi_8-\xi_6}N_{6,1}$	0		$\frac{6\xi-2}{2}N_{5,1}$	$\frac{6\xi-2}{2}N_{5,1}+\frac{5-6\xi}{2}N_{6,1}$	$\frac{5-6\xi}{2}N_{6,1}$	
I=6, p=2	$N_{6,2}=\frac{\xi-\xi_6}{\xi_8-\xi_6}N_{6,1}+\frac{\xi_9-\xi}{\xi_9-\xi_7}N_{7,1}$	0			$\frac{6\xi-3}{2}N_{6,1}$	$\frac{6\xi-3}{2}N_{6,1}+\frac{6-6\xi}{2}N_{7,1}$	$\frac{6-6\xi}{2}N_{7,1}$
I=7, p=2	$N_{7,2}=\frac{\xi-\xi_7}{\xi_9-\xi_7}N_{7,1}+\frac{\xi_{10}-\xi}{\xi_{10}-\xi_8}N_{8,1}$					$\frac{6\xi-4}{2}N_{7,1}$	$\frac{6\xi-4}{2}N_{7,1}+\frac{6-6\xi}{1}N_{8,1}$
I=8, p=2	$N_{8,2}=\frac{\xi-\xi_8}{\xi_{10}-\xi_8}N_{8,1}+\frac{\xi_{11}-\xi}{\xi_{11}-\xi_9}N_{9,1}$						$\frac{6\xi-5}{1}N_{8,1}$
I=0, p=3	$N_{0,3}=\frac{\xi-\xi_0}{\xi_3-\xi_0}N_{0,2}+\frac{\xi_4-\xi}{\xi_4-\xi_1}N_{1,2}$	$\frac{1-6\xi}{1}N_{1,2}$					
I=1, p=3	$N_{1,3}=\frac{\xi-\xi_1}{\xi_4-\xi_1}N_{1,2}+\frac{\xi_5-\xi}{\xi_5-\xi_2}N_{2,2}$	$6\xi N_{1,2}+\frac{2-6\xi}{2}N_{2,2}$	$\frac{2-6\xi}{2}N_{2,2}$				
I=2, p=3	$N_{2,3}=\frac{\xi-\xi_2}{\xi_5-\xi_2}N_{2,2}+\frac{\xi_6-\xi}{\xi_6-\xi_3}N_{3,2}$	$\frac{6\xi}{2}N_{2,2}+\frac{3-6\xi}{3}N_{3,2}$	$\frac{6\xi}{2}N_{2,2}+\frac{3-6\xi}{3}N_{3,2}$	$\frac{3-6\xi}{3}N_{3,2}$			

I=3, p=3	$N_{3,3}=\frac{\xi-\xi_3}{\xi_6-\xi_3}N_{3,2}+\frac{\xi_7-\xi}{\xi_7-\xi_4}N_{4,2}$	$\frac{6\xi}{3}N_{3,2}$	$\frac{6\xi}{3}N_{3,2}+\frac{4-6\xi}{3}N_{4,2}$	$\frac{6\xi}{3}N_{3,2}+\frac{4-6\xi}{3}N_{4,2}$	$\frac{4-6\xi}{3}N_{4,2}$
I=4, p=3	$N_{4,3}=\frac{\xi-\xi_4}{\xi_7-\xi_4}N_{4,2}+\frac{\xi_8-\xi}{\xi_8-\xi_5}N_{5,2}$	$\frac{6\xi-1}{3}N_{4,2}$	$\frac{6\xi-1}{3}N_{4,2}+\frac{5-6\xi}{3}N_{5,2}$	$\frac{6\xi-1}{3}N_{4,2}+\frac{5-6\xi}{3}N_{5,2}$	$\frac{5-6\xi}{3}N_{5,2}$
I=5, p=3	$N_{5,3}=\frac{\xi-\xi_5}{\xi_8-\xi_5}N_{5,2}+\frac{\xi_9-\xi}{\xi_9-\xi_6}N_{6,2}$	$\frac{6\xi-2}{3}N_{5,2}$	$\frac{6\xi-2}{3}N_{5,2}+\frac{6-6\xi}{3}N_{6,2}$	$\frac{6\xi-2}{3}N_{5,2}+\frac{6-6\xi}{3}N_{6,2}$	$\frac{6-6\xi}{3}N_{6,2}$
I=6, p=3	$N_{6,3}=\frac{\xi-\xi_6}{\xi_9-\xi_6}N_{6,2}+\frac{\xi_{10}-\xi}{\xi_{10}-\xi_7}N_{7,2}$	$\frac{6\xi-3}{3}N_{6,2}$	$\frac{6\xi-3}{3}N_{6,2}+\frac{6-6\xi}{2}N_{7,2}$	$\frac{6\xi-3}{3}N_{6,2}+\frac{6-6\xi}{2}N_{7,2}$	
I=7, p=3	$N_{7,3}=\frac{\xi-\xi_7}{\xi_{10}-\xi_7}N_{7,2}+\frac{\xi_{11}-\xi}{\xi_{11}-\xi_8}N_{8,2}$	$\frac{6\xi-4}{2}N_{7,2}$	$\frac{6\xi-4}{2}N_{7,2}+\frac{6-6\xi}{1}N_{8,2}$		
I=8, p=3	$N_{8,3}=\frac{\xi-\xi_8}{\xi_{11}-\xi_8}N_{8,2}+\frac{\xi_{12}-\xi}{\xi_{12}-\xi_9}N_{9,2}$	$(6\xi-5)N_{8,2}$			

Knot vector is given by

ξ_0	ξ_1	ξ_2	ξ_3	ξ_4	ξ_5	ξ_6	ξ_7	ξ_8	ξ_9	ξ_{10}	ξ_{11}	ξ_{12}
0	0	0	0	1/6	2/6	3/6	4/6	5/6	1	1	1	1

Control points along X-axis $\left(0 \quad \frac{1}{18} \quad \frac{1}{6} \quad \frac{2}{6} \quad \frac{3}{6} \quad \frac{4}{6} \quad \frac{5}{6} \quad \frac{17}{18} \quad 1\right)$

Control points along Y-axis $\left(0 \quad \frac{1}{18} \quad \frac{1}{6} \quad \frac{2}{6} \quad \frac{3}{6} \quad \frac{4}{6} \quad \frac{5}{6} \quad \frac{17}{18} \quad 1\right)$

The gauss points are as shown in Table 4.

Table 4

4 × 4 Gauss quadrature and the gauss points.

aa(1,1)=0.8611363116	*aa* (1,2)= 0.8611363116	*wg*(1,1)=0.3478548451	*wg* (1,2) = 0.3478548451
aa (2,1)=0.8611363116	*aa* (2,2) =-0.8611363116	*wg*(2,1)=0.3478548451	*wg* (2,2) = 0.3478548451
aa (3,1)=0.8611363116	*aa* (3,2) = 0.3399810436	*wg* (3,1)=0.3478548451	*wg* (3,2) = 0.6521451549
aa (4,1)= 0.8611363116	*aa* (4,2) = -0.3399810436	*wg* (4,1)=0.3478548451	*wg* (4,2) = 0.6521451549
aa (5,1)=-0.8611363116	*aa* (5,2)= 0.8611363116	*wg* (5,1)=0.3478548451	*wg* (5,2) = 0.3478548451
aa (6,1)=-0.8611363116	*aa* (6,2) =-0.8611363116	*wg* (6,1)=0.3478548451	*wg* (6,2) = 0.3478548451
aa (7,1)=-0.8611363116	*aa* (7,2) = 0.3399810436	*wg* (7,1)=0.3478548451	*wg* (7,2) = 0.6521451549
aa (8,1)=-0.8611363116	*aa* (8,2) = -0.3399810436	*wg* (8,1)=0.3478548451	*wg* (8,2) = 0.6521451549
aa (9,1)=0.3399810436	*aa* (9,2) = 0.8611363116	*wg* (9,1)=0.6521451549	*wg* (9,2) = 0.3478548451
aa (10,1)=0.3399810436	*aa* (10,2) =-0.8611363116	*wg* (10,1)=0.6521451549	*wg* (10,2) = 0.3478548451
aa (11,1)=0.3399810436	*aa* (11,2) = 0.3399810436	*wg* (11,1)=0.6521451549	*wg* (11,2)= 0.652145154
aa (12,1)=0.3399810436	*aa* (12,2) = -0.339981043	*wg* (12,1)=0.6521451549	*wg* (12,2) = 0.6521451549
aa (13,1)=-0.3399810436	*aa* (13,2) = 0.8611363116	*wg* (13,1)=0.6521451549	*wg* (13,2) = 0.3478548451
aa (14,1)=-0.3399810436	*aa* (14,2) =-0.8611363116	*wg* (14,1)=0.6521451549	*wg* (14,2) = 0.3478548451
aa (15,1)=-0.3399810436	*aa* (15,2) = 0.3399810436	*wg* (15,1)=0.6521451549	*wg* (15,2) = 0.6521451549
aa (16,1)=-0.3399810436	*aa* (16,2) = -0.339981043	*wg* (16,1)=0.6521451549	*wg* (16,2) = 0.6521451549

Table 5
The equivalent natural coordinates for the gauss points.

	$0.5*(\xi_{i+1}-\xi_i)\xi+(\xi_{i+1}+\xi_i)*0.5$	$0.5*(\eta_{j+1}-\eta_j)\eta+(\eta_{j+1}+\eta_j)*0.5$
1	$0.5*(\frac{1}{6})(0.8611363116)+0.5(\frac{1}{6})=0.1550946926$	$0.5*(\frac{1}{6})(0.8611363116)+0.5(\frac{1}{6})=0.1550946926$
2	$0.5*(\frac{1}{6})(0.8611363116)+0.5(\frac{1}{6})=0.1550946926$	$0.5*(\frac{1}{6})(-0.8611363116)+0.5(\frac{1}{6})=0.01157197403$
3	$0.5*(\frac{1}{6})(0.8611363116)+0.5(\frac{1}{6})=0.1550946926$	$0.5*(\frac{1}{6})(0.3399810436)+0.5(\frac{1}{6})=0.111665087$
4	$0.5*(\frac{1}{6})(0.8611363116)+0.5(\frac{1}{6})=0.1550946926$	$0.5*(\frac{1}{6})(-0.3399810436)+0.5(\frac{1}{6})=0.0550015797$
5	$0.5*(\frac{1}{6})(-0.8611363116)+0.5(\frac{1}{6})=0.01157197403$	$0.5*(\frac{1}{6})(0.8611363116)+0.5(\frac{1}{6})=0.1550946926$
6	$0.5*(\frac{1}{6})(-0.8611363116)+0.5(\frac{1}{6})=0.01157197403$	$0.5*(\frac{1}{6})(-0.8611363116)+0.5(\frac{1}{6})=0.01157197403$
7	$0.5*(\frac{1}{6})(-0.8611363116)+0.5(\frac{1}{6})=0.01157197403$	$0.5*(\frac{1}{6})(0.3399810436)+0.5(\frac{1}{6})=0.111665087$
8	$0.5*(\frac{1}{6})(-0.8611363116)+0.5(\frac{1}{6})=0.01157197403$	$0.5*(\frac{1}{6})(-0.3399810436)+0.5(\frac{1}{6})=0.0550015797$
9	$0.5*(\frac{1}{6})(0.3399810436)+0.5(\frac{1}{6})=0.111665087$	$0.5*(\frac{1}{6})(0.8611363116)+0.5(\frac{1}{6})=0.1550946926$
10	$0.5*(\frac{1}{6})(0.3399810436)+0.5(\frac{1}{6})=0.111665087$	$0.5*(\frac{1}{6})(-0.8611363116)+0.5(\frac{1}{6})=0.01157197403$
11	$0.5*(\frac{1}{6})(0.3399810436)+0.5(\frac{1}{6})=0.111665087$	$0.5*(\frac{1}{6})(0.3399810436)+0.5(\frac{1}{6})=0.111665087$
12	$0.5*(\frac{1}{6})(0.3399810436)+0.5(\frac{1}{6})=0.111665087$	$0.5*(\frac{1}{6})(-0.3399810436)+0.5(\frac{1}{6})=0.0550015797$
13	$0.5*(\frac{1}{6})(-0.3399810436)+0.5(\frac{1}{6})=0.0550015797$	$0.5*(\frac{1}{6})(0.8611363116)+0.5(\frac{1}{6})=0.1550946926$
14	$0.5*(\frac{1}{6})(-0.3399810436)+0.5(\frac{1}{6})=0.0550015797$	$0.5*(\frac{1}{6})(-0.8611363116)+0.5(\frac{1}{6})=0.01157197403$
15	$0.5*(\frac{1}{6})(-0.3399810436)+0.5(\frac{1}{6})=0.0550015797$	$0.5*(\frac{1}{6})(0.3399810436)+0.5(\frac{1}{6})=0.111665087$
16	$0.5*(\frac{1}{6})(-0.3399810436)+0.5(\frac{1}{6})=0.0550015797$	$0.5*(\frac{1}{6})(-0.3399810436)+0.5(\frac{1}{6})=0.0550015797$

Table 6
Basis functions at gauss points.

Basis functions N_i and M_i	0.1550946926	0.01157197403	0.111665087	0.0550015797
$N_{0,3}=(1-6\xi)*(1-6\xi)*(1-6\xi)N_{3,0}$	3.3471 x 10^{-4}	0.8058320	0.035940	0.30075023
$N_{1,3}=6\xi*(1-6\xi)*(1-6\xi)N_{3,0}+\frac{(2-6\xi)}{2}\left((6\xi(1-6\xi)N_{3,0}+6\xi\frac{(2-6\xi)}{2}N_{3,0})\right)$	0.30510371	0.187187	0.5162916	0.562845
$N_{2,3}=\frac{6\xi}{2}\left(6\xi*(1-6\xi)+\frac{(2-6\xi)}{2}*6\xi\right)N_{3,0}+\frac{3-6\xi}{3}\left(\frac{6\xi}{2}\right)6\xi N_{3,0}$	0.56025621	6.9243 x 10^{-3}	0.3976432	0.130414
$N_{3,3}=\frac{6\xi}{3}*\frac{6\xi}{2}*6\xi N_{3,0}$	0.13430534	5.5785 x 10^{-5}	0.050125	5.99 x 10^{-3}
	1.0000000	1.00000000	1.0000000	1.000000

Table 7
Basis functions in local coordinate system.

$$N_1 = (1-6\xi)*(1-6\xi)*(1-6\xi)N_{3,0}$$

$$N_2 = 6\xi*(1-6\xi)*(1-6\xi)N_{3,0} + \frac{(2-6\xi)}{2}\left((6\xi(1-6\xi)N_{3,0} + 6\xi\frac{(2-6\xi)}{2}N_{3,0})\right)$$

$$N_3 = \frac{6\xi}{2}\left(6\xi*(1-6\xi) + \frac{(2-6\xi)}{2}*6\xi\right)N_{3,0} + \frac{3-6\xi}{3}\left(\frac{6\xi}{2}\right)6\xi N_{3,0}$$

$$N_4 = \frac{6\xi}{3}*\frac{6\xi}{2}*6\xi\, N_{3,0}$$

$$M_1 = (1-6\eta)*(1-6\eta)*(1-6\eta)M_{3,0}$$

$$M_2 = 6\eta*(1-6\eta)*(1-6\eta)M_{3,0} + \frac{(2-6\eta)}{2}\left((6\eta(1-6\eta)M_{3,0} + 6\eta\frac{(2-6\eta)}{2}M_{3,0})\right)$$

$$M_3 = \frac{6\eta}{2}\left(6\eta*(1-6\eta) + \frac{(2-6\eta)}{2}*6\eta\right)M_{3,0} + \frac{3-6\eta}{3}\left(\frac{6\eta}{2}\right)6\eta M_{3,0}$$

$$M_4 = \frac{6\eta}{3}*\frac{6\eta}{2}*6\eta\, M_{3,0}$$

Table 8
The basis function for element #1.

Gauss point #1 - Basis function for Element #1		
Node #		
1	N1M1	3.3471 x 10^{-4} x 3.3471 x 10^{-4} = 1.120307 x 10^{-7}
2	N2M1	0.30510371 x 3.3471 x 10^{-4} = 1.0212 x e-4
3	N3M1	0.56025621 x 3.3471 x 10^{-4} = 1.875233 e-4
4	N4M1	0.13430534 x 3.3471 x 10^{-4} = 4.495334 e -5
10	N1M2	3.3471 x 10^{-4} x 0.30510371 = 1.02121 e-4
11	N2M2	0.30510371 x 0.30510371 = 0.09308827
12	N3M2	0.56025621 x 0.30510371 = 0.1709362482
13	N4M2	0.13430534 x 0.30510371 = 0.0409770
19	N1M3	3.3471 x 10^{-4} x 0.56025621 = 1.875233e-4
20	N2M3	0.30510371 x 0.56025621 = 0.1709362482
21	N3M3	0.56025621 x 0.56025621 = 0.31388702
22	N4M3	0.13430534 x 0.56025621 = 0.0752454
28	N1M4	3.3471 x 10^{-4} x 0.13430534 = 4.495334 e-5
29	N2M4	0.30510371 x 0.13430534 = 0.04097705
30	N3M4	0.56025621 x 0.13430534 = 0.0752454
31	N4M4	0.13430534 x 0.13430534 = 0.01803792
		Total = 1.00000000

Similarly at other gauss points, we can write the basis functions.

ξ = 0.1550946926 η = 0.1550946926

Table 9
The basis functions and its derivatives.

Basis functions and first derivatives	At Xi
$N_1 = (1-6\xi)*(1-6\xi)*(1-6\xi)N_{3,0}$ $M_1 = (1-6\eta)*(1-6\eta)*(1-6\eta)M_{3,0}$	3.347x10^{-4}
$\frac{dN_1}{d\xi} = 3(1-6\xi)^2(-6)N_{3,0}$, $\frac{dM_1}{d\eta} = 3(1-6\eta)^2(-6)M_{3,0}$	-0.086774
$\frac{d^2N_1}{d\xi^2} = (3)(2)(1-6\xi)(-6)(-6)N_{3,0}$, $\frac{d^2M_1}{d\eta^2} = (3)(2)(1-6\eta)(-6)(-6)M_{3,0}$	14.9973
$N_2 = 6\xi*(1-6\xi)*(1-6\xi)N_{3,0} + \frac{(2-6\xi)}{2}\left((6\xi(1-6\xi)N_{3,0} + 6\xi\frac{(2-6\xi)}{2}N_{3,0})\right)$	0.3051

$$M_2 = 6\eta * (1-6\eta) * (1-6\eta) M_{3,0} + \frac{(2-6\eta)}{2}\left((6\eta(1-6\eta) M_{3,0} + 6\xi \frac{(2-6\eta)}{2} M_{3,0}) \right)$$

$$\frac{dN_2}{d\xi} = \begin{pmatrix} 6\xi * 2 * (1-6\xi) * (-6) + (1-6\xi)^2(6) + (1-3\xi)(6)(1-6\xi) + (1-3\xi)(-6)(6\xi) + (6\xi)(-3)(1-6\xi) + \\ (1-3\xi)^2(6) + 6\xi(2)(1-3\xi)(-3) \end{pmatrix} N_{3,0}$$

$$\frac{dM_2}{d\eta} = \begin{pmatrix} 6\eta * 2 * (1-6\eta) * (-6) + (1-6\eta)^2(6) + (1-3\eta)(6)(1-6\eta) + (1-3\eta)(-6)(6\eta) + (6\eta)(-3)(1-6\eta) + \\ (1-3\eta)^2(6) + 6\eta(2)(1-3\eta)(-3) \end{pmatrix} M_{3,0}$$

-4.97303

$$\frac{d^2N_2}{d\xi^2} = 12(1-6\xi)(-6) + (6)(-12)(1-6\xi) + 12(1-6\xi)(-6) + (-6)(6)(1-3\xi) + (6)(1-6\xi)(-3) - 36(1-3\xi) -$$
$$36(-3)(\xi) - 18\xi(-6) - 18(-6\xi) + 12(-3)(1-3\xi) - 36(1-3\xi) - 36\xi(-3)$$

$$\frac{d^2M_2}{d\eta^2} = 12(1-6\eta)(-6) + (6)(-12)(1-6\eta) + 12(1-6\eta)(-6) + (-6)(6)(1-3\eta) + (6)(1-6\eta)(-3) - 36(1-3\eta) -$$
$$36(-3)(\eta) - 18\eta(-6) - 18(-6\eta) + 12(-3)(1-3\eta) - 36(1-3\eta) - 36\eta(-3)$$

27.7548

$$N_3 = \frac{6\xi}{2}\left(6\xi * (1-6\xi) + \frac{(2-6\xi)}{2} * 6\xi \right) N_{3,0} + \frac{3-6\xi}{3}\left(\frac{6\xi}{2} \right) 6\xi N_{3,0}$$

$$M_3 = \frac{6\eta}{2}\left(6\eta * (1-6\eta) + \frac{(2-6\eta)}{2} * 6\eta \right) M_{3,0} + \frac{3-6\eta}{3}\left(\frac{6\eta}{2} \right) 6\eta M_{3,0}$$

0.56025

$$\frac{dN_3}{d\xi} = \left(\frac{36\xi^2}{2}(-6) + (1-6\xi)(36\xi) + \frac{36\xi^2}{2}(-3) + (1-3\xi)(36\xi) + \frac{36\xi^2}{2}(-2) + 36\xi(1-2\xi) \right) N_{3,0}$$

$$\frac{dM_3}{d\eta} = \left(\frac{36\eta^2}{2}(-6) + (1-6\eta)(36\eta) + \frac{36\eta^2}{2}(-3) + (1-3\eta)(36\eta) + \frac{36\eta^2}{2}(-2) + 36\eta(1-2\eta) \right) M_{3,0}$$

2.4619347

$$\frac{d^2N_3}{d\xi^2} = \begin{pmatrix} \frac{(36)(2)\xi}{2}(-6) + (1-6\xi)(36) + (-6)(36\xi) + \frac{(36)(2)\xi}{2}(-3) + (-3)(36\xi) + (1-3\xi)(36) + \frac{(36)(2)\xi}{2}(-2) + \\ 36\xi(-2) + 36(1-2\xi) \end{pmatrix} N_{3,0}$$

$$\frac{d^2M_3}{d\eta^2} = \begin{pmatrix} \frac{(36)(2)\eta}{2}(-6) + (1-6\eta)(36) + (-6)(36\eta) + \frac{(36)(2)\eta}{2}(-3) + (-3)(36\eta) + (1-3\eta)(36) + \frac{(36)(2)\eta}{2}(-2) + \\ 36\eta(-2) + 36(1-2\eta) \end{pmatrix} M_{3,0}$$

-76.2525

$$N_4 = \frac{6\xi}{3} * \frac{6\xi}{2} * 6\xi\, N_{3,0}$$

$$M_4 = \frac{6\eta}{3} * \frac{6\eta}{2} * 6\eta\, M_{3,0}$$

0.134303

$$\frac{dN_4}{d\xi} = 36 * 3 * \xi^2 N_{3,0}$$

$$\frac{dM_4}{d\eta} = 36 * 3 * \eta^2 M_{3,0}$$

2.597871

$$\frac{d^2N_4}{d\xi^2} = 36 * 3 * 2 * \xi\, N_{3,0}$$

$$\frac{d^2M_4}{d\eta^2} = 36 * 3 * 2 * \eta\, M_{3,0}$$

33.5

Table 10
Control point coordinates for element #1.

	X	*Y*
N1	0	0
N2	0.055555555555556	0
N3	0.166666666666667	0
N4	0.333333333333333	0
N10	0	0.055555555555556
N11	0.055555555555556	0.055555555555556

N12	0.166666666666667	0.055555555555556
N13	0.333333333333333	0.055555555555556
N19	0	0.166666666666667
N20	0.055555555555556	0.166666666666667
N21	0.166666666666667	0.166666666666667
N22	0.333333333333333	0.166666666666667
N28	0	0.333333333333333
N29	0.055555555555556	0.333333333333333
N30	0.166666666666667	0.333333333333333
N31	0.333333333333333	0.333333333333333

For gauss point #1

Table 11
Derivatives for element #1.

$\frac{dN_1}{d\xi}\frac{dM_1}{d\eta}$	0.00752973710746563	$\frac{dN_9}{d\xi}\frac{dM_9}{d\eta}$	-0.213632070617073
$\frac{dN_2}{d\xi}\frac{dM_2}{d\eta}$	0.431530165929331	$\frac{dN_{10}}{d\xi}\frac{dM_{10}}{d\eta}$	-12.2432804180917
$\frac{dN_3}{d\xi}\frac{dM_3}{d\eta}$	-0.213632070617073	$\frac{dN_{11}}{d\xi}\frac{dM_{11}}{d\eta}$	6.06112284463265
$\frac{dN_4}{d\xi}\frac{dM_4}{d\eta}$	-0.225427832419724	$\frac{dN_{12}}{d\xi}\frac{dM_{12}}{d\eta}$	6.39578964407610
$\frac{dN_5}{d\xi}\frac{dM_5}{d\eta}$	0.431530165929331	$\frac{dN_{13}}{d\xi}\frac{dM_{13}}{d\eta}$	-0.225427832419724
$\frac{dN_6}{d\xi}\frac{dM_6}{d\eta}$	24.7310472396657	$\frac{dN_{14}}{d\xi}\frac{dM_{14}}{d\eta}$	-12.9192969875034
$\frac{dN_7}{d\xi}\frac{dM_7}{d\eta}$	-12.2432804180917	$\frac{dN_{15}}{d\xi}\frac{dM_{15}}{d\eta}$	6.39578964407610
$\frac{dN_8}{d\xi}\frac{dM_8}{d\eta}$	-12.9192969875034	$\frac{dN_{16}}{d\xi}\frac{dM_{16}}{d\eta}$	6.74893517584699

$\frac{dx}{d\xi}$	$\frac{dy}{d\xi}$	$\frac{dx}{d\eta}$	$\frac{dy}{d\eta}$	$\frac{d^2x}{d\xi^2}$	$\frac{d^2x}{d\eta^2}$	$\frac{d^2y}{d\xi^2}$	$\frac{d^2y}{d\eta^2}$	$\frac{d^2x}{d\xi d\eta}$	$\frac{d^2y}{d\xi d\eta}$
1	0	0	1	0	0	0	0	0	0

For gauss point #1

Table 12
Second derivatives for element #1.

	Value		Value		Value		Value
$\frac{d^2N_1}{d\xi^2}M_1$	0.00501	$\frac{d^2N_1}{d\xi^2}M_2$	4.57572	$\frac{d^2N_1}{d\xi^2}M_3$	8.40231	$\frac{d^2N_1}{d\xi^2}M_4$	2.01421
$\frac{d^2N_2}{d\xi^2}M_1$	0.00928	$\frac{d^2N_2}{d\xi^2}M_2$	8.46808	$\frac{d^2N_2}{d\xi^2}M_3$	15.5497	$\frac{d^2N_2}{d\xi^2}M_4$	3.72761
$\frac{d^2N_3}{d\xi^2}M_1$	-0.02552	$\frac{d^2N_3}{d\xi^2}M_2$	-23.2649	$\frac{d^2N_3}{d\xi^2}M_3$	-42.7209	$\frac{d^2N_3}{d\xi^2}M_4$	-10.241
$\frac{d^2N_4}{d\xi^2}M_1$	0.01121	$\frac{d^2N_4}{d\xi^2}M_2$	10.2211	$\frac{d^2N_4}{d\xi^2}M_3$	18.7688	$\frac{d^2N_4}{d\xi^2}M_4$	4.4992

	Value		Value		Value		Value
$\frac{d^2M_1}{d\eta^2}N_1$	0.005019	$\frac{d^2M_2}{d\eta^2}N_1$	0.00928	$\frac{d^2M_3}{d\eta^2}N_1$	-0.02552	$\frac{d^2M_4}{d\eta^2}N_1$	0.01121
$\frac{d^2M_1}{d\eta^2}N_2$	4.57572	$\frac{d^2M_2}{d\eta^2}N_2$	8.46808	$\frac{d^2M_3}{d\eta^2}N_2$	-23.2649	$\frac{d^2M_4}{d\eta^2}N_2$	10.2211
$\frac{d^2M_1}{d\eta^2}N_3$	8.40231	$\frac{d^2M_2}{d\eta^2}N_3$	15.5497	$\frac{d^2M_3}{d\eta^2}N_3$	-42.7209	$\frac{d^2M_4}{d\eta^2}N_3$	18.7688
$\frac{d^2M_1}{d\eta^2}N_4$	2.01421	$\frac{d^2M_2}{d\eta^2}N_4$	3.72761	$\frac{d^2M_3}{d\eta^2}N_4$	-10.241	$\frac{d^2M_4}{d\eta^2}N_4$	4.49929

	1	2	3	4	5	6	7	8	9	10	11	12	13	14	15	16
d^2N/dx^2	0.005	0.0093	-0.0255	0.0112	4.5757	8.4681	-23.2649	10.2211	8.4023	15.5498	-42.7209	18.7688	2.0142	3.7276	-10.2411	4.4993
d^2N/dy^2	0.005	4.5757	8.4023	2.0142	0.0093	8.4681	15.5498	3.7276	-0.0255	-23.2649	-42.7209	-10.2411	0.0112	10.2211	18.7688	4.4993
$d^2N/dxdy$	0.0075	0.4315	-0.2136	-0.2254	0.4315	24.731	-12.2433	-12.9193	-0.2136	-12.2433	6.0611	6.3958	-0.2254	-12.9193	6.3958	6.7489

REFERENCES

[1] Punmia B.C., Designs R.C.C., 2006, *Laxmi Publications*, ISBN: 9788131809426.

[2] Liang Q.Q., 1999, Topology optimisation of strut-and-tie models in non-flexural reinforced concrete members, *International Conference on Mechanics of Structures*, *Materials and Systems*, Wollongong, Australia.

[3] Leu L.-J., 2006, Strut and tie methodology for three dimensional reinforced concrete structures, *Journal of Structural Engineering* **132**(6): 929-938.

[4] Michelle A.G.M., 1904, LVIII the limits of economy of material in frame-structures, *Philosophical Magazine* **8**(47): 589-597.

[5] Khajehzadeh M., 2011, Modified particle swarm optimization for optimum design of spread footing and retaining wall, *Journal of Zhejiang University-Science A* **12**(6): 415-427.

[6] James B., 2005, *A Finite Element Approach to Reinforced Concrete Slab Design*, Master of Science Thesis, Georgia Institute of Technology.

[7] Kwak H.G., Filippou F.C., 1992, Finite element analysis of reinforced concrete structures under monotonic and cyclic loads, *Earthquake Engineering, Tenth World Conference*, Rotterdam.

[8] Kaveh A., Behnam A.F., 2013, Design optimisation of reinforced concrete 3D structures considering frequency constraints via., a charged system search, *Scientia Iranica A* **20**(3): 387-396.

[9] Kim H., Baker G., 2011, *Topology Optimisation of Reinforced Concrete Structures*, School of Engineering, University of Warwick.

[10] Oded A., 2013, A topology optimisation procedure for reinforced concrete structures, *Computers & Structures* **114-115**: 46-85.

[11] Oded A., Michael B., 2010, Topology optimisation for conceptual design of reinforced concrete structures, *9th World Congress on Structural and Multidisciplinary Optimization*, Shizuoka, Japan.

[12] Oded A., Ole S., 2013, Reinforcement layout design for concrete structures based on continuum damage and truss topology optimisation, *Structural and Multidisciplinary Optimization* **47**: 157-174.

[13] Liang Q.Q., 2000, Topology optimisation of strut-and-tie models in reinforced concrete structures using an evolutionary procedure, *ACI Structural Journal* **97**: 322-332.

[14] Sarma K., Adeli H., 1998, Cost optimisation of concrete structures, *Journal of Structural Engineering* **124**(5): 570-578.

[15] Babiker S., 2012, Design optimisation of reinforced concrete beams using artificial neural network, *International Journal of Engineering Inventions* **1**(8): 07-13.

[16] Guerra A., Kiousis P.D., 2006, Design optimisation of reinforced concrete structures, *Computers and Concrete* **3**(5): 313-334.

[17] Singh B., Rai H.S., 2014, Optimisation of rcc beam, *International Journal of Engineering, Business and Enterprise Applications* **14**: 21-34.

[18] Kaveh A., Sabzi O., 2012, Optimal design of reinforced concrete frames using big bang-big crunch algorithm, *International Journal of Civil Engineering*, *Structural Engineering* **10**(3): 189-200.

[19] Yousif S.T., 2013, Optimum cost design of reinforced concrete continuous beams using genetic algorithms, *International Journal of Applied Sciences and Engineering Research* **12**(4): 681-693.

[20] McCarthy T.J., McCluskey S., 2009, A particle swarm optimisation approach to reinforced concrete beam design according to AS360, *Proceedings on the First International Conference on Soft Computing Technology in Civil, Structural and Environmental Engineering, Civil-Comp Press*, Stirlingshire, UK.

[21] Karthiga N., 2014, Finite element analysis of reinforced concrete beams, *International Journal of Innovative research in Advanced Engineering* **1**(8): 272-285.

[22] Chandrasekhar K.N.V., Sahithi N.S.S., 2018, A step by step illustrative procedure to perform isogeometric analysis and find the nodal displacements for a two dimensional plate structure, *i-Managers Journal on Structural Engineering* **6**: 40-52.

[23] Chandrasekhar K.N.V., Sahithi N.S.S., 2018, A step by step procedure to perform isogeometric analysis of beam and bar problems in civil engineering including sizing optimisation of a beam, *i-Managers Journal on Structural Engineering* **7**: 13-27.

[24] Sahithi N.S.S., Chandrasekhar K.N.V., 2019, Isogeometric topology optimisation of continuum structures using evolutionary algorithms, *Journal of Applied Computational Mechanics* **5**: 414-440.

[25] Sairam K.S., Sinha P.K., 1991, Hygrothermal effects on the bending characteristics of laminated composite plates, *Computers & Structures* **40**(4): 1009-1015.

[26] Kant T., Swaminathan K., 2001, Analytical solutions for free vibration of laminated composite and sandwich plates based on a higher-order refined theory, *Composite Structures* **53**: 73-85.

[27] Hughes T.J.R., 2010, Efficient quadrature for NURBS-based isogeometric analysis, *Computer Methods in Applied Mechanical and Engineering* **199**: 301-313.

[28] Hassani B., 2012, An isogeomtrical approach to structural topology optimisation by optimality criteria, *Structural and Multidisciplinary Optimization* **45**: 223-233.

[29] Benson D.J., 2011, A large deformation, rotation-free, isogeometric shell, *Computer Methods in Applied Mechanical and Engineering* **200**: 1367-1378.

[30] Hoang X., Nguyena E.A., Nguyen-Xuan H., Thuc P.V., 2017, Geometrically nonlinear isogeometric analysis of functionally graded microplates with the modified couple stress theory, *Computers and Structures* **193**: 110-127.

[31] Dufour J.-E., 2018, A cost-effective isogeometric approach for composite plates based on a stress recovery procedure, *Composites Part B* **138**: 12-18.

[32] Valizadeh N., 2013, NURBS-based finite element analysis of functionally graded plates: Static bending, vibration, buckling and flutter, *Composite Structures* **99**: 309-326.

[33] Wang X., 2015, Isogeometric finite element method for buckling analysis of generally laminated composite beams with different boundary conditions, *International Journal of Mechanical Sciences* **104**: 190-199.

[34] Somireddy M., Rajagopal A., 2014, Meshless natural neighbor Galerkin method for the bending and vibration analysis of composite plates, *Composite Structures* **111**: 138-146.

[35] Weeger O., 2014, Nonlinear frequency response analysis of structural vibrations, *Computational Mechanics* **54**: 1477-1495.

[36] Patton A., 2019, Fast and accurate elastic analysis of laminated composite plates via. isogeometric collocation and an equilibrium-based stress recovery approach, *Composite Structures* **225**: 111026.

[37] Shojaee S., 2012, Free vibration and buckling analysis of laminated composite plates using the NURBS-based isogeometric finite element method, *Composite Structures* **94**: 1677-1693.

[38] Behshad A., Ghasemi M.R., 2014, NURBS-IGA modelling: analysis and optimisation of laminated plates, *Tehnicki Vjesnik* **21**(4): 789-797.

[39] Hong Ch., 2013, A rotation-free isogeometric analysis for composite sandwich thin plates, *International Journal of Composite Materials* **3**(6A): 10-18.

[40] Farshad R., Roger S., 2016, Isogeometric nonlinear shell elements for thin laminated composites based on analytical thickness integration, *Journal of Micromechanics and Molecular Physics* **01**(03-04): 1640010.

[41] Shuang Q., 2018, Multilevel optimisation of laminated composite thin-walled structures using isogeometric analysis, *13th World Congress on Computational Mechanics* (WCCM XIII), New York, NY, USA.

[42] Kapoor H., 2013, *Isogeometric Finite Element Code Development for Analysis of Laminated Composite Structures*, Ph.D. Thesis, Virginia Institute.

[43] Gupta A., Ghosh A., 2019, NURBS-based thermo-elastic analyses of laminated and sandwich composite plates, *Sådhanå* **44**: 84.

[44] Cassanova C.F., 2014, *Analysis of Composite Shells: Isogeometric Modelling and Damage Identification*, Ph.D. Thesis, Universidad de Granada.

[45] Kiendl J.M., 2011, *Isogeometric Analysis and Shape Optimal Design of Shell Structures*, Ph.D. Thesis, Technische Universität München.

[46] Tran L.V., 2013, An isogeometric finite element formulation for thermal buckling analysis of functionally graded plates, *Finite Element Analysis and Design* **70**: 65-76.

[47] Tran L.V., 2013, *Isogeometric Analysis for Functionally Graded Plates Using Higher Order Shear Deformation Theory*, *Universiteit Gent*.

[48] Breitenberger M., 2013, Isogeometric layout optimisation of shell structures using trimmed NURBS surfaces, *10th World Congress on Structural Multidisciplinary Optimisation*, Orlando, USA.

[49] Deng X., 2015, Isogeometric analysis of continuum damage in rotation-free composite shells, *Computer Methods in Applied Mechanical and Engineering* **284**: 349-372.

[50] Kiani Y., 2018, NURBS-based isogeometric thermal postbuckling analysis of temperature dependent graphene reinforced composite laminated plates, *Thin-Walled Structures* **125**: 211-219.

[51] PavanG.S., Nanjunda Rao K.S., 2016, Analysis of laminated composite plates using isogeometric collocation method, *Eccomas Congress 2016*, *VII European Congress on Computational Methods in Applied Sciences and Engineering*, Crete Island, Greece.

[52] Liu H., 2018, Isogeometric analysis based topology optimization design with global stress constraint, *Computer Methods in Applied Mechanical and Engineering* **342**: 625-652.

[53] Civalek O., Yavas A., 2006, Large deflection static analysis of rectuangular plates on two parameter elastic foundations, *International Journal of Science & Technology* **1**(1): 43-50.

[54] Civalek O., Kiracioglu O., 2010, Free vibration analysis of Timoshenko beams by DSC method, *International Journal for Numerical Methods in Biomedical Engineering* **26**: 1890-1898.

[55] Akgöz B., Civalek O., 2017, A size-dependent beam model for stability of axially loaded carbon nanotubes surrounded by Pasternak elastic foundation, *Composite Structures* **176**: 1028-1038.

[56] Wu H., Yang J., Kitipornchai S., 2017, Parametric instability of Thermo-mechanically loaded functionally graded graphene reinforced nanocomposite plates, *International Journal of Mechanical Sciences* **135**: 431-440.

[57] Shen H-S., Xiang Y., Fan Y., Hui D., 2017, Nonlinear vibration of functionally graded graphene-reinforced composite laminated cylindrical panels resting on elastic foundations in thermal environments, *Composites Part B* **136**: 177-186.

[58] Hsu M.H., Hsu Y.L., 2005, Generalization of two- And three-dimensional structural topology optimization, *Engineering Optimization* **37**: 83-102.

[59] Hughes T.J.R., 2005, Isogeometric analysis: CAD, finite elements, NURBS, exact geometry and mesh refinement, *Computer Methods in Applied Mechanical and Engineering* **194**: 4135-4195.

[60] Liang Q.Q., 2002, Performance based optimisation for strut-and-tie modeling of concrete, *Journal of Structural Engineering* **128**(6): 815.

[61] Behshad A., Ghasemi M.R., 2013, Isogeometric based modelling and analysis of laminated composite plates under transverse loading, *Journal of Solid Mechanics* **5**(4): 380-390.

[62] Hong Ch., Pierre S., Bordas A., 2014, Isogeometric analysis of laminated composite and sandwich plates using a new inverse trigonometric shear deformation theory, *European Journal of Mechanics / A solids* **43**: 89-108.

[63] Serdyuk D., 2012, *Fundamentals of Optimization Problems*, FAU Erlangen-Nürnberg, TU München, Uni Stuttgart.

[64] Tang P-S., Chang K-H., 2001, Integration of topology and shape optimisation for design of structural components, *Structural and Multidisciplinary Optimization* **22**: 65-82.

[65] Chirehdast M., Gea H.Ch., 1992, Further advances in the integrated structural optimisation system, *American Institute of Aeronautics and Astronautics* **4817**: 974-981.

[66] Hassani B., 2012, An isogeometrial approach to structural topology optimisation by optimality criteria, *Structural and Multidisciplinary Optimization* **45**: 223-233.

[67] Hong Ch., Nguyen-Xuan H., Bordas S.P.A., Nguyen-Thanh N., Rabczuk T., 2015, Isogeometric analysis of laminated composite plates using the higher-order shear deformation theory, *Mechanics of Advanced Materials and Structures* **22**: 451-469.

[68] Liang Q.Q., 2007, Performance-based optimisation: A Review, *Advances in Structural Engineering* **109**(6): 739-753.

[69] Austin J., Thomas C., Hughes J.R., Bazilevs Y., 2009, *Isogeometric Analysis Toward Integration of CAD and FEA*, John Wiley & Sons.

[70] Hervandil M., Anna S., Fonseca J.S.O., 2002, Topology optimisation of continuum two-dimensional structures under compliance and stress constraints, *Mecanica Computacional* **XXI**: 2732-2751.

[71] Abolbashari M.H., Keshavarzmanesh Sh., 2006, On various aspects of application of the evolutionary optimisation method for 2D and 3D continuum structures, *Finite Elements in Analysis and Design* **42**: 478-491.

[72] Yang X.Y., Xie Y.M., Steven G.P., 2005, Evolutionary methods for topology optimisation of continuous structures with design dependent loads, *Computers & Structures* **83**: 956-963.

[73] Kant T., Swaminathan K., 2002, Analytical solutions for the static analysis of laminated composite and sandwich plates based on a higher order refined theory, *Composite Structures* **56**: 329-344.